DENTATE NETWORK ACTIVITY IS NECESSARY FOR SPATIAL WORKING MEMORY BY SUPPORTING CA3 SHARP-WAVE RIPPLE GENERATION AND PROSPECTIVE FIRING OF CA3 NEURONS

Takuya Sasaki[1,2,3,4], **Verónica C. Piatti**[1,4], **Ernie Hwaun**[1], **Siavash Ahmadi**[1], **John E. Lisman**[5], **Stefan Leutgeb**[1,6], and **Jill K. Leutgeb**[1,7]

[1]Neurobiology Section and Center for Neural Circuits and Behavior, Division of Biological Sciences, University of California, San Diego, USA

[2]Laboratory of Chemical Pharmacology, Graduate School of Pharmaceutical Sciences, University of Tokyo, Japan

[3]Precursory Research for Embryonic Science and Technology, Japan Science and Technology Agency, Japan

[5]Department of Biology, Brandeis University, USA

[6]Kavli Institute for Brain and Mind, University of California, San Diego, USA

Abstract

Complex spatial working memory (WM) tasks have been shown to require both hippocampal sharp wave ripple (SWR) activity and dentate gyrus (DG) neuronal activity. We therefore asked whether DG inputs to CA3 contribute to spatial WM by promoting SWR generation. Recordings from DG and CA3 while rats performed a dentate-dependent WM task on an 8-arm radial maze revealed that the activity of dentate neurons and the incidence rate of SWRs both increased during reward consumption. We then found reduced reward-related CA3 SWR generation without direct input from dentate granule neurons. Furthermore, CA3 cells with place fields in not-yet visited arms preferentially fired during SWRs at reward locations, and these prospective CA3 firing patterns were more pronounced for correct trials and were dentate dependent. These results

[7]Corresponding Author. Address: 9500 Gilman Dr., MC 0357, University of California, San Diego, La Jolla, CA 92093. jleutgeb@ucsd.edu.
[4]These authors contributed equally to the work

indicate that coordination of CA3 neuronal activity patterns by DG is necessary for the generation of neuronal firing patterns that support goal-directed behavior and memory.

Working memory (WM) is the ability to temporarily store and process information that is relevant for completing goal-directed actions. Based on the profound behavioral performance deficits in complex spatial WM tasks after dentate gyrus (DG) lesions, the projections of DG granule cells to CA3 through the mossy fiber (MF) pathway have been considered to be critical for WM with delays of tens of seconds to hours[1]. The finding that spatial firing patterns of dentate cells show pattern separation[2,3] has led to the suggestion that DG projections to CA3 support memory by promoting the generation of distinct hippocampal firing patterns. However, the DG-CA3 network is also characterized by recurrent connections, both directly between CA3 cells as well as more indirectly between dentate granule cells, hilar mossy cells, and CA3 cells[4,5]. These dense direct and indirect recurrent pathways in the dentate-CA3 network form associative circuits, which have been suggested to be critical for retaining complex spatial WM[6, 7].

Furthermore, the CA3 region – independently[8,9] or by modulation from the CA2 region[10] – is thought to initiate sharp-wave ripples (SWRs), which then propagate from CA3 to CA1. SWRs are prominent hippocampal network oscillations (150–250 Hz) that are observed during sleep as well as during periods of immobility in awake behavior[11]. SWRs are characterized by short bouts of increased neuronal activity during which time-compressed sequences are replayed, which correspond to sequential activity patterns that are observed on a longer time scale in behavior[12–16]. The reactivation of sequential activity patterns during SWRs is thought to underlie processes important for memory such as consolidation and retrieval[17–19]. In particular, it has been shown that selective elimination of awake SWRs in hippocampus impairs future route planning[20] and behavioral performance in a spatial WM task[21]. This suggests that SWR-associated reactivation of hippocampal cell ensembles during ongoing behavior is a potential mechanism for maintaining representations of stored items for use in planning future choices in WM.

There is evidence that SWRs do not occur during periods of low DG granule cell activity[22] and, conversely, that CA3 and hilar neuronal activity is increased in parallel during SWRs[8–10,23,24]. These correlations, together with the findings that SWRs and dentate inputs to CA3 are both critical for spatial WM, led us to investigate whether DG inputs to CA3 may contribute to spatial WM by effects on SWR generation and on ripple-related neuronal firing patterns. In a task in which DG is necessary for WM performance, we therefore recorded neuronal firing patterns in DG and CA3 and examined to what extent CA3 network activity patterns and ripple-associated firing patterns of individual CA3 cells were dependent on DG inputs.

RESULTS

Dentate granule neurons were necessary for spatial WM in the 8-arm radial maze

We first confirmed that our version of the spatial WM task was dependent on the DG. Rats ($n = 16$) were trained to perform an 8-arm radial maze task in which reward was available at

the end of each of the arms (Fig. 1a). In the first phase of each trial, four arms were sequentially presented in a pseudorandom order (forced phase). In the second phase, all arms were made accessible such that the animal had to remember and choose the arms where reward was still available (choice phase). The optimal strategy is to visit each arm only once per trial. A trial with at least one reentry into an arm was therefore considered an incorrect trial. Initial training on the task was performed for 30 min (6–10 trials) per day until at least 50 % of trials were correct over 5 consecutive days (days to criterion: 15.1 ± 2.4, n = 16 animals; Fig. 1b and Supplementary Fig. 1a). After reaching criterion, dentate granule cells were selectively lesioned with bilateral infusions of colchicine (six sites per hemisphere, see Online Methods)[1] throughout the entire septo-temporal axis of the hippocampus in 11 of the 16 animals (Fig. 1c). The remaining five animals underwent sham surgery and served as controls. In the lesioned rats (n = 11), there was a 73.7 ± 1.4 % (range: 59.0 % to 82.4 %) reduction of the volume in the DG granule cell layer, as quantified using the Cavalieri method (Supplementary Fig. 1c and 1d).

During behavioral testing after surgery, control animals performed the majority of all trials without errors (n = 30 days from 5 animals, $64.3 \% \pm 3.8$ correct). In contrast to the high level of performance of control rats, all animals with DG lesions showed a striking deficit in their ability to choose correct arms (% correct trials, range over 6 days: 18.4 % to 45.3 % in 11 DG-lesioned rats vs 39.6 % to 78.2 % in 5 control rats, $F_{(1,70)} = 16.07$, $P = 1.3 \times 10^{-3}$; Fig. 1b; number of errors: range over 6 days: 2.5 to 1.0 in 11 DG-lesioned rats vs 1.5 to 0.3 in 5 control rats, $F_{(1,70)} = 6.55$, $P = 0.023$, repeated measures ANOVA over six days after surgery; Supplementary Fig. 1a). Some errors were already committed during the first choice after the forced phase (0.03 ± 0.01 errors per choice in control and 0.18 ± 0.04 in DG-lesioned rats), but the likelihood of errors increased for later choices (4th choice: 0.11 ± 0.02 errors per choice in control and 0.26 ± 0.03 in DG-lesioned rats) when a higher number of previous choices needed to be remembered (Supplementary Fig. 1b). Despite the difference in overall error levels, control and lesion rats therefore appeared to use a strategy for which the number of past choices increased the likelihood of future errors. Furthermore, we confirmed that damage to the entire CA1 and CA3 was not substantial (21.3 ± 2.9 % and 12.1 ± 1.9 %, respectively) in DG-lesioned rats. While damage to dorsal CA1 and CA3 (31.9 ± 3.6 % and 19.6 ± 2.1 %) was larger compared to ventral damage (6.4 ± 5.6 % and 8.7 ± 3.5 %), neither dorsal nor ventral damage were correlated with spatial memory performance in DG-lesioned rats (Supplementary Fig. 1c).

Dentate cells were selectively active at reward locations

To examine neuronal firing patterns that may contribute to spatial WM performance, we recorded DG cells in 8 rats during the WM task ($n = 71$ cells, including 24 cells from the granule cell layer and 47 from the hilus; Fig. 2a–b and Supplementary Fig. 2). As previously reported, we found that many active dentate cells (> 0.01 Hz, $n = 62$ of 71) had spatially selective activity patterns on maze arms or the center platform (22.6 %, 14 of 62 cells). The proportion of spatially-selective cells during WM approximately corresponded to the proportion identified during random foraging (RF) on the 8-arm maze (30.6 %, 15 of 49 active cells) although field locations did not match between the tasks (Supplementary Fig. 3a). Consistent with recent reports[25–27], place-selectivity was more typical for DG cells

recorded from sites in the hilus compared to the granule cell layer (Fig. 2c–e). In addition to standard spatial firing on the maze, we also observed in WM that the firing rates of many dentate cells were higher on arm ends than in the inner portion of the maze (> 1.5 fold more active: 37 of 62 cells, 59.7 %; median: 6.9-fold; Fig. 2c). Arm-end selectivity could occur either on a limited set of arm ends (spatially selective; 23 of 37 cells; Fig. 2d and e) or without a consistent arm preference (14 of 37 cells). Arm-end selective firing was most typical for recording sites located in the dentate granule cell layer. Therefore, the firing patterns of the majority of active DG cells in WM differed substantially from those of standard place cells.

Because dentate cells recorded in the granule cell layer fired predominantly at the reward locations in the spatial WM task, we examined the precise pattern of dentate spiking in more detail and recorded an additional 16 arm-end selective dentate cells (in 2 rats) with sensors that signaled precisely when rats were licking the reward (Fig. 2f). For all analysis of reward-related neuronal activity patterns, only the initial visit to each of the eight arms was included and repeat visits were excluded. Dentate cells with firing rates > 0.01 Hz (12/16, mean rate: 0.022 ± 0.016 Hz) showed activity that was on average 18.4-fold higher after contact compared to before contact with the reward (range: 4.4 to 69.5 fold). Throughout the approximately 3 s long period while rats consumed the reward, average dentate firing rates increased gradually (Fig. 2g).

SWRs in CA3 preferentially occurred at reward locations

We then examined whether the increased DG activity during reward periods in WM was associated with distinct CA3 LFP patterns. We began by evaluating the running speed in different sections of the maze and found that periods of immobility and low running velocities only occurred on the arm ends (Fig. 3a–c). This region of the maze was characterized by SWRs (Fig. 3d–f), which preferentially occurred during the period while rats consumed the reward ($n = 4$ control rats, during reward: 0.151 ± 0.023 Hz; during immobility before and after reward: 0.042 ± 0.012 Hz and 0.071 ± 0.009 Hz, respectively; $n = 17$ tetrodes, reward vs immobility before: t(16) = 4.00, $P = 0.0020$; reward vs immobility after: t(16) = 5.10, $P = 2.2 \times 10^{-4}$, paired t tests; Fig. 3g–h and Supplementary Fig. 4–8). The reward-related increase in incidence rate was observed irrespective of the amplitude threshold for SWRs (from > 3 SD to > 5 SD; Supplementary Fig. 5). Furthermore, the incidence rate of ripples at reward sites was higher during correct compared to incorrect trials for the choice but not the forced phase of the task (choice, correct: 0.16 ± 0.02 Hz, incorrect: 0.12 ± 0.02 Hz, t(16) = 2.13, $P = 0.049$, paired t test; forced, correct: 0.18 ± 0.03 Hz, incorrect: 0.20 ± 0.02 Hz, t(16) = 0.92, $P = 0.37$, paired t test; Supplementary Fig. 9b). More frequent reward-associated CA3 ripples during the choice phase were thus correlated with more accurate WM processing.

To evaluate whether SWRs at reward locations qualitatively corresponded to awake ripples, we confirmed that the firing rates of individual CA3 cells were low before ripple events and increased several-fold during ripple events ($n = 116$ cells, before: 0.13 ± 0.02 Hz, during: 0.73 ± 0.14 Hz; Fig. 3i and Supplementary Fig. 7e). Such transient surges in hippocampal

firing rates from a low baseline level correspond to patterns that have previously been reported for SWRs during wakefulness and sleep[9,10,28–30].

Dentate network activity was necessary for reward-associated increases in CA3 SWRs

To more directly investigate whether the reward-related increase in CA3 SWRs and CA3 neuronal activity depended on dentate inputs, we performed dorsal CA3 recordings in 4 control and 10 DG-lesioned rats (Fig. 4a–f and Supplementary Fig. 10). Even though our DG lesion size was substantial along the entire dorsoventral extent of the DG, we scored the extent of remaining MF innervation at each CA3 recording location based on TIMM-positive signals in the CA3 striatum lucidum (Fig. 4b; scores from 0 to 4: no detectable density, low density, moderate density, near-complete density, and control density; see Online Methods for a detailed description). For analysis of electrophysiological signals, sites with scores of 0–1 were combined into the low-density MF input (lMF) group and sites with scores of 2 were the high-density MF input (hMF) group. There were no CA3 recording sites in lesioned rats with a score higher than 2.

We first confirmed that DG-lesions did not result in any differences in behavioral patterns in the spatial WM task, including the time spent at the reward location (Fig. 4c and Supplementary Table 1). We next observed that reward-related SWR rates were reduced at many, but not all CA3 recording sites (Fig. 4d–f) and therefore tested whether the heterogeneous effects could be explained by the degree of residual MF projections. At lMF sites, SWRs did not show the typical increase in incidence rates during the reward period, while hMF sites showed an increase in SWRs during the reward period comparable to control CA3 sites (range for control sites: 63 % to 328 %, median = 235 %; range for lMF sites: 0 % to 252 %, median = 101 %; range for hMF sites: 80 % to 388 %, median = 169 %; control vs lMF, U = 453, Z = 3.95, $P = 7.9 \times 10^{-5}$; control vs hMF, U = 262, Z = 1.18, P = 0.24, Mann-Whitney U test; Fig. 4e and see Supplementary Fig. 9c–e for additional detail). The lack of reward-related increase in SWR rates was also observed for the raw ripple rates at lMF sites ($n = 20$ tetrodes; F(2,57) = 0.42, $P = 0.42$, ANOVA; Fig. 4f). Differences between low and high-density MF groups were apparent even within a single DG-lesioned animal (Supplementary Fig. 9f), but differences depending on remaining CA1 volume, CA3 volume, or recording location within CA3 were not observed (Supplementary Fig. 11). In addition, we analyzed high-frequency oscillations during rest and found that SWRs were affected to a similar extent as those at reward locations (Supplementary Fig. 12).

Reward-associated 20–50 Hz oscillations at CA3 recording sites were DG dependent

To determine whether reward-related oscillations other than SWRs were affected by DG lesions, CA3 LFP spectrograms were further analyzed. In control recordings, we found that fast gamma (65–140 Hz) power was low at reward sites compared to oscillations in the 20–50 Hz band, which sharply increased during reward consumption ($n = 17$ tetrodes; reward vs all other behavior, $P < 0.01$, Scheffé test; Fig. 5a, 5c–e, and Fig. 3e). The power increase in the 20–50 Hz band was significantly greater when associated with reward than while the animals simply paused without taking reward (reward: 0.28 ± 0.04, immobility at arm end: 0.06 ± 0.04, control, t(16) = 8.91, $P = 5.8 \times 10^{-8}$, paired t test; Supplementary Fig. 4f) and could thus not be explained by the onset of immobility[31]. In addition, LFP coherence

between DG and CA3 selectively increased in the 20–50 Hz band during reward consumption ($n = 35$ tetrode pairs, reward vs all other behavior: $P < 0.01$, Scheffé test; Fig. 5b), consistent with the possibility that these oscillations in CA3 depended on intact dentate granule cells or that the signal was volume conducted from DG to CA3. We found that the reward-associated increase in 20–50 Hz power was significantly lower at lMF recording sites in DG-lesioned animals compared to control animals (control: $n = 17$ tetrodes, range: 0.04 to 1.06, median = 0.48; hMF: $n = 10$ tetrodes, range: –0.10 to 0.66, median = 0.17; lMF: $n = 20$ tetrodes, range: –0.31 to 0.70, median = 0.24; control vs hMF, U = 288, Z = 2.49, $P = 0.26$; control vs lMF, U = 431, Z = 3.28, $P = 2.0 \times 10^{-4}$, Mann-Whitney U test followed by posthoc Bonferroni corrections; Fig. 5f–i).

The increase in both 20–50 Hz power and SWR rates at reward sites in controls, along with the dentate dependence of both types of oscillations, raised the question whether these oscillations were coupled. Contrary to evidence for coupling, we found that 20–50 Hz oscillations and SWRs occurred mostly during separate phases of reward consumption. A transient bout of 20–50 Hz oscillations occurred during the first ~0.5 s after the reward encounter while the incidence of SWRs began to increase after 0.5 s and was highest ~1–2 s after the first contact with the reward (Fig. 5a and 5c). Furthermore, the two types of oscillations were related to DG and CA3 firing rates in opposite directions (Fig. 5c). DG and CA3 firing rates were low during 20–50 Hz oscillations and then gradually increased with increasing SWR occurrence.

Dentate network activity was necessary for reward-associated increases in CA3 firing

The finding that dentate activity and CA3 SWR rates gradually increased at reward locations and that MF inputs to CA3 were required for SWR generation suggested that DG inputs may contribute to spatial WM by modulating CA3 neuronal activity patterns at reward locations. We therefore focused on further examining CA3 network activity and its dependence on DG MF inputs. An increase in CA3 pyramidal cell firing during reward-related SWRs was found for control but not for lMF sites (control vs lMF, medians: 242 % vs 46 %, U = 3624, Z = 2.37, $P = 0.018$, Mann-Whitney U test; Supplementary Fig. 8c). The lower CA3 firing rates during ripple events, along with the reduced frequency of reward-associated ripples (Fig. 4f), can be expected to jointly result in a prominent reduction in the overall number of CA3 spikes at CA3 sites without MF inputs. Taken together, direct MF inputs from DG granule cells are thus necessary for the generation of reward-associated increases in CA3 SWRs and neuronal firing rates.

The dentate-dependent increase in CA3 SWRs was memory related

We next asked whether the increase in CA3 SWRs was invariably related to reward consumption or may be modulated by WM processing in association with reward consumption, as would be suggested by the finding that effects of DG lesions are particularly pronounced in complex spatial WM tasks[1] and by our finding that SWR rates are particularly high during correct trials. To address this question, we performed recordings on the linear track, where rats retrieved rewards without needing to use spatial memory (Supplementary Fig. 13). On the linear track, SWR dynamics did not differ between lMF,

hMF, and control sites (Supplementary Fig. 13i). These findings suggest that only memory-related SWR increase is dentate dependent.

Spatial firing patterns of CA3 cells were compromised by DG lesions

After identifying a substantial effect of DG inputs on reward-associated CA3 firing in WM, we next examined whether MF projections also contributed to spatial firing patterns of CA3 place cells (n = 116 control, 49 hMF, and 57 lMF cells; Fig. 6) and to the relation between spatial and reward-related firing (Fig. 7 and see Supplementary Fig. 14 for additional examples). We first examined how many active CA3 cells we could identify at each of the recording sites. At lMF sites, the number of active cells per tetrode was significantly lower than in controls (range and median for control sites: 2 to 13 and 6; hMF sites: 0 to 9 and 6; lMF sites: 0 to 7 and 2; control vs hMF: U = 250.5, Z = 0.61, P > 0.99; control vs lMF: U = 443.5, Z = 3.70, P = 4.2×10^{-4}, Mann-Whitney U test followed by posthoc Bonferroni corrections; Fig. 6b), but firing rates of each of the recorded cells were significantly higher (range and median for control sites: 0.00 Hz to 1.21 Hz and 0.07 Hz; hMF sites: 0.00 Hz to 3.14 Hz and 0.16 Hz; lMF sites: 0.00 Hz to 2.88 Hz and 0.19 Hz; control vs lMF: D_{max} = 0.30, P = 0.0024; control vs hMF: D_{max} = 0.20; P = 0.11, Kolmogorov-Smirnov test; Fig. 6c) than at control sites. The lesion data suggest that the removal of MF inputs to CA3 altered CA3 network sparsity and excitability such that fewer CA3 cells are active but with each active cell firing at a higher rate.

Analysis of the spatial firing patterns was then performed for CA3 cells with an average firing rate of > 0.05 Hz during the spatial WM task (control, n = 64 cells; hMF, n = 34 cells; lMF, n = 47 cells). In the control group, 50.0 % and 27.8 % of active CA3 neurons had a place field on either a single arm or on the stem, respectively. Together, more than 75 % of active CA3 cells thus had detectable fields on the maze. Furthermore, recordings in the RF task on the same maze on the same day showed that CA3 place cells had similar spatial maps of the environment between the spatial WM and RF task (Supplementary Fig. 3b). Field locations in CA3 were therefore predominantly determined by spatial location rather than by task demands, as previously reported[32]. The spatial firing of control CA3 cells during WM was then compared to cells from DG-lesioned rats during WM. While place fields were generally larger and more dispersed with dentate lesions, the reduced spatial stability of CA3 firing after DG lesions occurred at all CA3 recording sites regardless of the degree of MF reduction (Fig. 6c and 6d, see figure legends for statistics). This differs from the effects on reward-associated CA3 firing which were directly dependent on the degree of remaining MF inputs to a particular recording site.

Prospective firing of CA3 place cells during reward periods depended on direct input from the dentate gyrus

In awake SWRs, sequences of place-specific neurons are replayed in both prospective and retrospective manners[13–16]. To examine out-of-field reactivation patterns of CA3 cells at the reward locations in the spatial WM task, we selected CA3 cells with place fields preferentially on a single arm of the radial maze (control, n = 39 cells; lMF, n = 22 cells) and analyzed out-of-field spikes that occurred at reward locations on arms other than the arm with the place field (Fig. 7a and 7b). We first confirmed that most reward-associated out-of-

field spikes occurred in close temporal association with SWRs (Fig. 7c) and then analyzed when these spikes occurred throughout the series of arm entries in each trial. For each cell and each trial, reward-associated spikes before entering the arm with the place field were considered prospective, and spikes after exiting the arm with the field were defined as retrospective (Fig. 7b and 7d). In the control group, reward-associated prospective CA3 firing rates were significantly higher than retrospective firing rates (prospective: 0.15 ± 0.02 Hz, retrospective: 0.08 ± 0.01 Hz, t(38) = 3.57, $P = 9.8 \times 10^{-4}$, paired t test; Fig. 7f). The higher likelihood for prospective firing is consistent with a tendency for a decrease in reward-associated firing rates over the time throughout a trial (Supplementary Fig. 15a). For quantification of the relative strength of prospective compared to retrospective firing, a ratio between these rates was defined for individual cells (difference divided by the sum). The prospective ratio ranged between −1 and +1, with a higher positive value reporting stronger bias toward prospective firing. The average prospective ratio in the spatial WM task was 0.34 ± 0.07 (Fig. 7f) indicating that firing during reward consumption preferentially included cells with place fields on arms that had not yet been visited within the trial. At lMF recording sites, no difference was observed between reward-associated prospective and retrospective firing rates (prospective: 0.38 ± 0.07 Hz, retrospective: 0.32 ± 0.05 Hz, t(21) = 0.97, $P = 0.34$, paired t test; Fig. 7d and 7f), and the prospective ratio was significantly lower than in the control group (control: 0.34 ± 0.07, lMF: 0.05 ± 0.08, t(59) = 2.60, $P = 0.012$, Student's t test; Fig. 7f). Similarly, preferential prospective firing in the control but not in the lMF group was also observed when restricting the analysis to only spikes that occurred during SWR events that were detected on the same recording electrode as the spikes (control: prospective, 0.67 ± 0.13 Hz, retrospective, 0.35 ± 0.08 Hz, t(38) = 2.15, $P = 0.038$, paired t test; lMF: prospective, 0.37 ± 0.13 Hz, retrospective, 0.35 ± 0.09 Hz, t(21) = 0.70, $P = 0.49$, paired t test; Fig. 7e and 7g), but the difference of prospective ratios between the two groups no longer reached significance with the smaller sample size (control: 0.22 ± 0.10, lMF: -0.09 ± 0.13, t(59) = 1.86, $P = 0.068$, t test; Fig. 7g). These results suggest that hippocampal representation of future locations in the spatial WM task occurred during reward periods during the spatial WM task and that the emergence of these reward-related firing patterns in the CA3 circuit is supported by direct MF inputs from dentate granule neurons.

If the SWRs and the associated prospective neuronal signals support the planning of future trajectories, then these activity patterns should be relevant to behavioral performance[33]. Accordingly, prospective firing at control recording sites was observed on correct trials but not incorrect trials (Supplementary Fig. 16). Interestingly, prospective firing also emerged at lMF sites during correct, but not incorrect trials (correct: prospective, 0.43 ± 0.08 Hz, retrospective, 0.26 ± 0.04 Hz, t(20) = 2.80, $P = 0.011$; incorrect: prospective, 0.37 ± 0.08 Hz, retrospective, 0.35 ± 0.07 Hz, t(20) = 0.31, $P = 0.76$, paired t test; Supplementary Fig. 16d). These results suggest that prospective neuronal signals predict successful behavioral performance and that even CA3 networks with only minor remaining DG inputs generate prospective coding on occasions when animals are more likely to make correct decisions. While we found that additional firing patterns of CA3 cells, such as phase locking to theta and gamma oscillations were also reduced by DG legions, we did not find that phase locking differed between correct and incorrect trials in either lesioned or control rats (Supplementary

Fig. 17), which suggests that these effects are less directly related to ongoing WM performance.

DISCUSSION

The DG is the first processing stage in the hippocampal trisynaptic circuit, and its contribution to intrahippocampal processing is thought to be particularly critical when two or more closely related items need to be retained in memory. Previous studies have therefore investigated the ability of dentate cells to separate similar input patterns by generating distinct patterns of neuronal activity, with a particular focus on pattern separation by distinct spatial firing patterns[2,3]. However, complex spatial WM tasks have been found to not only require dentate granule neurons[34] but also hippocampal SWRs[21], and we therefore asked whether the role of the dentate cells in memory may extend beyond pattern separation. We began by confirming that selective lesions of the dentate gyrus impaired spatial WM and then used the same task for recording neural activity in intact and DG-lesioned rats. While we found standard place fields for a subset of dentate cells, as previously reported, we also identified a large proportion of cells with very low average firing rates (< 0.1 Hz). These cells would in standard spatial analysis be considered silent[35,36], but consistently fired at one or more reward locations. The increased firing of dentate cells at reward locations was preceded by a brief 20–50 Hz oscillation and occurred in parallel with an increase in CA3 SWR and neuronal activity. Furthermore, it was predominantly CA3 cells with place fields on not-yet visited arms that were active on the arm ends over the course of each trial. Lesions of dentate granule neurons precluded the increase of CA3 SWRs and of prospective CA3 neuronal activity at the reward site. Taken together, these findings reveal a role of dentate computations beyond pattern separation and suggest that the dentate gyrus is necessary for the generation of neuronal firing patterns that support goal-directed behavior.

Novel type of non-spatial firing of dentate granule cells

The focus of previous work has been on spatial firing patterns of dentate cells and proposed a role in pattern separation of these firing patterns with the suggestion that multi-peaked spatial cells are particularly well suited to discriminate between input patterns[2,3,37]. Recently, multi-peaked spatial firing patterns were found to be typical for hilar mossy cells while dentate granule cells had either single fields or were silent during behavior[25–27]. Our analysis of firing patterns of dentate cells is consistent with these results, but also identifies a new role for sparsely active dentate granule cells (~65 %), which would be considered silent in standard spatial analysis. We found that these cells could become selectively active at the arm ends during reward consumption. For many of these cells, the activity was not at a single reward location in the maze, but rather at multiple reward locations over a series of trials, and the same cells rarely had standard place fields on the maze. In addition, detailed analysis of the behavioral pattern at the reward location revealed that dentate activity at the reward location peaked about 0.5–1 s after the reward consumption commenced. Together with the spatial WM deficits after selective dentate granule cell lesions, these findings therefore suggest that the activity of a large proportion of dentate cells after the onset of reward consumption is necessary for spatial WM computations. These computations could

include the tagging of the current reward location as a no longer valid target or the selection of a not-yet visited location on the maze as the next target.

20–50 Hz oscillations at the onset of the reward period

Because we hypothesized that the updating of spatial WM is a computation that could be performed by circuits that include loops between the DG and the hippocampal CA3 region, we asked whether the dentate activity during the reward period was associated with oscillatory patterns and increased neuronal activity in CA3. While we found a striking increase in both 20–50 Hz as well as in SWRs during reward consumption, we found that these oscillatory events were largely non-overlapping. Immediately after reward encounter, a brief (< 0.5 s) bout of pronounced 20–50 Hz oscillations emerged, while the incidence of SWRs peaked during the later period of reward consumption in parallel with the increase in dentate firing.

Oscillation frequencies between 20–50 Hz include frequency bands that have been previously referred to as slow gamma, 20–40 Hz, and beta oscillations[38]. However, the occurrence of reward-related 20–50 Hz oscillations in CA3 while neuronal activity is low would preclude that these oscillations are directly corresponding to either 20–40 Hz oscillations or slow gamma, which have been reported selectively in CA1 or along with CA3 activation, respectively[39–43]. Even though beta oscillations in the dentate subregion have previously been described as evoked by cue encounters[44,45], our 20–50 Hz oscillations at reward were much more prominent in the spatial WM task compared to the linear track. If our oscillations were therefore of a similar mechanistic origin as cue-related beta oscillations, they would have been substantially amplified by memory processing.

Furthermore, none of the previous studies examined the lack of entrainment of either DG or CA3 networks that we found here, and our reward-related 20–50 Hz oscillations in DG and CA3 occurred while firing rates in both neuronal populations were at a minimum. The finding that these oscillations were nonetheless DG-dependent raises the possibility that the oscillations predominantly reflect synaptic currents that are evoked by afferent inputs to the dentate-CA3 network or by afferent inputs to the dentate and volume conduction to CA3, which would be diminished by degeneration of the target cell population. An additional possibility is that the DG lesion precluded the activation of local interneurons that coordinate the synchrony of the oscillations between the dentate and CA3 dendritic regions.

Dentate granule neuron activity was necessary for increased CA3 firing and sharp wave ripple generation during reward consumption

The parallel increase of dentate activity, CA3 activity, and CA3 SWRs following the initial contact with the reward, along with the strong inputs of DG to CA3, suggested that DG inputs were required for activating CA3 during reward-associated immobility. We directly tested this prediction by performing lesions of the DG granule cells and found a substantial attenuation of the increase in CA3 SWRs during the period of contact with the reward. Interestingly, DG lesions did not result in a general decrease of CA3 activity but rather resulted in an elevated average firing rate of CA3 cells during theta periods, as previously reported[46]. While this may be a compensatory response that could also result in larger CA3

fields, the inputs from DG to CA3 were specifically required for eliciting brief bouts of CA3 SWRs after reward encounter in the spatial WM task while DG-lesion effects were not observed on the linear track. These results suggest that DG is specifically required for a memory-related elevation in CA3 activity. In addition, the difference between WM and the linear track is consistent with the possibility that there are both dentate-dependent and dentate-independent SWRs in CA3, as previously reported in slice experiments[47].

DG participated in biasing arm-end CA3 activity towards not-yet visited spatial locations

Given that CA3 neuronal activity and CA3 SWRs were selectively increased throughout reward consumption, we examined whether reward-related neuronal activity may be informative for successfully completing the spatial WM task. As each trial progressed, CA3 cells with place fields on not-yet-visited arms fired preferentially during reward consumption, as if CA3 performed a look-ahead towards possible future target locations. Consistent with the suggestion that such prospective coding may be necessary for guiding future choices, we found that look-ahead CA3 activity was more pronounced during correct compared to incorrect trials and that the WM deficits after DG lesions were accompanied by a loss of prospective coding. DG lesions therefore did not only attenuate the emergence of SWRs at the arm ends but concurrently also reduced the information content of the remaining SWRs. It is also interesting to note that prospective coding tended to reemerge in correct trials in DG-lesioned rats. Remaining mossy fiber inputs to CA3 were, in the many incorrect trials, thus not sufficient for generating prospective coding. However, when prospective coding was occasionally generated, its occurrence was associated with a higher likelihood for a trial to be completed correctly.

The relation between spatial WM performance and representing future locations during reward consumption raises the question how neuronal activity that points to future locations could subsequently result in the realization of successful movement sequences. This type of progression has been implemented for theta sequences in computational models[7], and recent experimental work has shown that the information content of SWRs and theta-sequences is related[48]. We therefore hypothesize that intrahippocampal networks can generate continuity between non-theta and theta states, which allows for preferential prospective activity during CA3 SWRs to contribute to the selection of particular theta sequences. The selection could either be mediated by a strong feed forward signal from dentate to CA3 or by loops that engage the associational projections from CA3 back to DG. Irrespective of how the computation is implemented in the DG-CA3 network, our data show that the DG and, in particular, the non-spatial DG firing patterns after contact with the reward, are a critical component of neuronal computations that support spatial WM. Taken together, we found a new type of firing pattern of otherwise silent dentate neurons and show that the dentate gyrus supports an increase in CA3 SWRs and CA3 prospective activity patterns during the period after contact with the reward, suggesting a role for dentate activity in SWR generation and goal selection. Computations of the dentate gyrus are thus not limited to pattern separation, but are also more directly involved in organizing memory-guided behavior.

ONLINE METHODS

Approvals

All surgical and experimental procedures were approved by the Institutional Animal Care and Use Committee at the University of California, San Diego, and conducted at the University of California, San Diego according to National Institutes of Health guidelines.

Subjects

A total of 37 male Long Evans rats (3–6 months old) were used in this study. The animals were housed individually and maintained on a 12-h light/12-h dark schedule with lights off at 6:00 AM. All animals were obtained from Charles River Laboratory. Following at least 1 week of adaptation to the laboratory, access to food was restricted and the rats were maintained at about 85 % of free-feeding body weight. Water was readily available.

Sixteen animals were trained in a spatial working memory (WM) task and used for behavioral testing before and after either a dentate lesion (n = 11) or sham surgery (n = 5). Twenty animals were used for recordings in the WM task. Ten of these animals received a surgery during which a chronic electrophysiological recording assembly was implanted, and 10 animals received both an implant and a dentate lesion. On days with recordings, 16 animals (7 control and 9 lesioned) first performed the WM task and next performed a random foraging (RF) task. Four animals performed only the WM task. After recordings in the WM task for at least three days, 6 recording animals (3 control and 3 lesioned) performed a linear track task. One additional animal with a recording assembly and dentate lesion performed only the linear track task. Control and lesioned animals from the same litters were assigned randomly, and tested experimentally in parallel.

Spatial working memory (WM) task on the radial 8-arm maze

All behavioral training occurred in the rats' dark phase. Rats were trained on a semiautomated black Plexiglas 8-arm radial maze with a central circular platform (27 cm diameter) and 8 arms (79 cm × 12 cm) to which access was controlled by a remote switch. First, daily 10-min habituation sessions with immediate access to all 8 arms were performed until the rat ate the chocolate milk reward (0.2 ml) at the end of each arm. In the next training stage, each trial started with access to all arms initially restricted. After an interval of 2 min, the experimenter made the first arm available and then sequentially presented one arm at a time up to the 4th arm (forced phase). The sequences during the forced phase were pseudorandom excluding instances in which all 4 arms would have been presented in spatial order such as 1, 2, 3, and 4. Immediately after the forced phase, all 8 arms were presented simultaneously (choice phase). During the choice phase, the animal was expected to visit the remaining four baited arms, and reentries into previously visited arms were considered errors. A trial ended when the rat had retrieved the reward from all 8 arms and returned to the central platform, or if the total time exceeded 10 min. When a trial was stopped for exceeding the time limit, it was removed from analysis. After an intertrial interval of 2 min, the next trial was initiated. Each day the rat was trained to perform 6–10 trials within 30 min a day and training was continued until the percentage of correct trials (i.e., trials without any

errors) over 5 consecutive days exceeded 50 %. After reaching the learning criterion, rats received either a selective DG lesion and/or a chronic recording implant.

Testing resumed 8 to 18 days after surgery on the same radial 8-arm maze in which the animals were pretrained. For animals without electrophysiological recording, at least 8 days of postsurgical testing were performed. For animals with electrophysiological recording, the animals were connected to a headstage and lightweight multiwire tether (see Electrode turning below) during testing after surgery, but the behavioral procedures were otherwise identical to presurgical training. Postsurgical testing was repeated daily until the animal performed at least 4 trials within 30 min a day regardless of the number of correct trials. Of 10 control animals, 6 animals required 1 day and 4 animals required 2 days to reach the criterion. Of 10 DG-lesioned animals, 8 and 2 animals required 1 and 3 days to reach this criterion, respectively. After reaching this post-surgery criterion, training continued together with electrophysiological data collection. Behavioral procedures were identical to those without recordings except that the rats were required to perform 10–20 trials per day within a period of 60 min. Recordings were performed for at least four days.

Animal position and electrophysiological data were sampled using a digital Neuralynx recording system with a multichannel head-mounted preamplifier[2]. Differential recordings were performed with a dedicated reference electrode in the cortex. Unit recordings were filtered at 600 Hz to 6 kHz, and spike waveforms above an amplitude of 40 µV were time-stamped and recorded at 32 kHz for 1 ms. LFP recordings were filtered between 1 and 425 Hz. Sufficient common mode rejection to eliminate muscle artifacts in LFP recordings was confirmed by finding that ripple amplitude during immobility at reward was as weakly correlated as for sleep SWRs (Supplementary Fig. 6a and 6b). Despite the weak correlation of ripple amplitudes across recording channels we also found coherence of high frequency events across tetrodes (Supplementary Fig. 6c and 6d). The period during which the rat licked the chocolate milk reward was detected by a wire sensor which detected contact of the rat with the milk on each of the individual arms. The sensor detected the switch from an open ended recording configuration to animal ground, and signals from these wires were digitized and timestamped by the Neuralynx recording system.

Distinct periods within a single trial of WM behavior were defined by the position and movement of the rat on the maze: (i) stem, < 36 cm from the maze center, (ii) outward, running outward in arm regions between 36–83 cm from the maze center, (iii) arm end 1, > 83 cm from the maze center prior to reward consumption, (iv) reward, contact with reward sensors, (v) arm end 2, > 83 cm from the maze center following the reward consumption period, and (vi) inward, running inward in arm regions between 36–83 cm from the maze center. For dentate recordings without reward sensors, periods iii–v were not analyzed separately. For illustration in figures, periods were normalized to the average of the period, and data from each trial were aligned according to their relative time within the period (Fig. 2f, 3g, 4d, 5b, 5d, and 5g, and Supplementary Figure 5). For all analysis of neuronal activity patterns, only the initial visit to each of the eight arms was included and repeat visits were excluded (all excluded data are discussed in the associated Life Science Reporting Summary).

Surgical procedures

In all 37 animals, a single surgery was performed that included (1) bilateral intracranial infusions of colchicine or vehicle into the dorsal and ventral dentate gyrus, and/or (2) chronic implantation of a tetrode array above the right hippocampus. At the time of surgery, the rat was anesthetized with isoflurane gas [2–2.5 % in O_2 (20 mL /1 L per minute)] and buprenorphine (0.05 mg/kg, s.c.) was given as an analgesic. For the DG lesion group, colchicine (2.5 mg/ml in phosphate buffer 0.1 M, pH 7.2) was injected into six sites (0.04 μl per site over 3 min) along the rostro-caudal axis of the dentate gyrus in each hemisphere at the following coordinates posterior of bregma, lateral of bregma, and ventral from dura (in mm): (1) −2.8, ±0.9, and −3.7; (2) −4.0, ± 2.1, and −3.6; (3) −5.2, ±3.2, and −3.7; (4) −5.2, ±3.2, and −7.6 mm; (5) −6.2, ±4.2, and −3.7; (6) −6.2, ±4.2, and −6.2 mm. Infusions were made using a 1-μl Hamilton syringe, and the injection needle was left in place for at least 5 min to prevent spread. Colchicine has previously been shown to cause selective cell death of dentate granule cells[49–51]. For the sham group, the same amount of the vehicle (phosphate buffer 0.1 M, pH 7.2) was injected into the same brain regions with the same procedure. In 21 animals, an electrode assembly that consisted of 14 independently movable tetrodes was implanted above the right hippocampus (control group: 4.0 mm posterior and 2.7–2.9 mm lateral to bregma or 6.1 mm posterior and 4.2–4.6 mm lateral to bregma; DG lesion group; 3.5–4.4 mm posterior and 2.8–3.2 mm lateral to bregma). Tetrodes were constructed as previously described[52]. Before surgery, tetrode tips were plated with platinum in order to lower electrode impedances to 150–300 kΩ at 1 kHz. The recording device was secured to the skull using stainless steel screws and dental cement.

Electrode turning

Rats were connected to the recording equipment via AC-coupled unity-gain operational amplifiers close to the rat's head while resting on a towel in a large pot on a pedestal. One tetrode remained in the cortex as a reference, and another tetrode was lowered to the stratum lacunosum-moleculare to record hippocampal local field potentials. The remaining 12 tetrodes were advanced to the CA3 cell layer in the DG-lesioned animals or to the CA3 cell layer and the DG cell layer in control animals over a period of at least 2 weeks after surgery. The depth profile of the LFP was used as a guide for electrode movement. When the tetrodes approached the cell layer, further movement of the tetrodes was completed in small increments over several days. Once the tetrodes were adjacent to the cell layer, as indicated by the presence of low-amplitude multiunit activity, tetrodes were not turned again and were allowed to settle into the cell layer for stable recordings over a period of many days. Tetrode recording locations were confirmed postmortem. DG lesions resulted in substantial tissue loss within DG which shifted the coordinates for CA3 recording sites and reduced the yield compared to controls.

Random foraging (RF) task

Seven control animals and 9 DG-lesioned animals performed a random foraging (RF) task on the radial arm maze. After completion of the WM task, the rat was allowed to rest for 5–20 min during which the floor of the maze was cleaned with water. The rat was then allowed

to freely forage for randomly scattered cocoa puffs for 10 min on the entire maze. The RF task was performed at least once a day and repeated for at least 2 consecutive days.

Linear track task

After completing electrophysiological recordings in the WM and RF tasks, 3 control animals and 3 DG-lesioned animals were tested on a linear track in a different room. One DG-lesioned animal was subject to only the linear track task. Animals were trained to run back and forth on a linear track (148×7 cm with shallow side walls rising 0.5 cm above the surface of the arm, 53 cm elevated from the floor) to obtain chocolate milk reward at the ends of the track for 3–4 10-min sessions with an intertial interval of 5 min. Sensors at each reward site indicated when the reward was consumed, as described for the WM task.

Behavioral periods were divided and defined as follows: (i) to reward, movement toward reward between the center and > 20 cm from an arm end, (ii) track end 1, < 20 cm from an arm end before reward, (iii) reward, contact with reward sensor, (iv) track end 2, < 20 cm from the end after reward, and (v) from reward, > 20 cm from the arm end to center of arm. For illustration in figures, each period was normalized to the average for the period, and data from each trial were aligned according to their relative time within the normalized period (Supplementary Fig. 13f and 13g).

Sharp-wave ripple detection

Sharp waves co-occur with ripples near the cell layer[11,22]. For the detection of ripples, LFP signals were band-pass filtered at 150–250 Hz and the root mean-square power was calculated in the ripple-band with a bin size of 10 ms. The threshold for awake-ripple detection was set to 3–5 standard deviations (SDs) above the mean[17]. Onset and offset of ripples was marked at the points when the ripple power first exceeded and dropped below 3 SDs above the mean, and events with a duration of < 15 ms were excluded. To calculate incidence rates for each behavioral period (e.g. reward), the total number of ripples was divided by the average duration of the corresponding period over all trials. In addition, the ripple rate during reward consumption in the WM task was also compared to the ripple rates during the immobility period at arm ends before and after reward consumption (defined as running speed < mean running speed during reward; Fig. 4e and Supplementary Fig. 9d). The ripple rate during reward consumption was normalized by ripple rates at track ends before reaching the reward on the linear track (Supplementary Fig. 13i).

LFP spectrum analysis

To compute the time-frequency representation of LFP power, LFP signals were convolved by a Morlet wavelet family defined by a constant ratio of $f_0/\sigma_f = 7$, where f_0 represents the frequency of interest and σ_f is the bandwidth of the wavelet in the frequency domain. The absolute power spectrum of the LFP during each 1 ms time window was calculated, and z-scores were computed for each frequency band using the mean and standard deviation of the power measured across the entire behavioral session for each tetrode. For constructing the representative behavior-related LFP power spectra in Fig. 3e, 5b, and Supplementary Figure 7a–b, the original time-frequency LFP power spectra were stretched or compressed in time, such that they matched the average time the animal spent in the different behavioral periods

(e.g., reward) over the entire session. The normalized data were then averaged across all trials. Oscillations in the gamma band were divided into the 20–50 Hz range and mid/fast gamma range (65–140 Hz). A 20-Hz cut-off was used to avoid confounds with theta harmonics (14–18 Hz), but to include frequency bands that have been referred to as 20–40 Hz or beta[43–45]. Because we found that the firing rates of CA3 cells were low during 20–50 Hz oscillations in the reward zone, we considered these oscillations mechanistically different from CA3-generated slow gamma oscillations, and refer to these oscillations by their frequency band. For quantification of each frequency band, the z-scored power was averaged separately for each behavioral state. To estimate the relationship between running speed and oscillations, z-scored power of each frequency and the velocity of animals were calculated during each 300 ms time window.

Coherence between two electrodes was computed using a multitaper method from the Chronux Matlab toolbox (http://chronux.org/) with a window size of 0.5 s and 5 tapers. For quantification, across behavioral periods data were averaged across all DG-CA3 pairs.

Spike sorting

Spike sorting was performed offline using a modified version of the graphical cluster-cutting software MClust[53]. Sleep recordings before and after the behavioral paradigms were included in the analysis to assure recording stability throughout the experiment and to identify hippocampal cells that were silent during behavior. Auto-correlation and cross-correlation functions were used as additional separation criteria. CA3 cells with an average firing rate of less than 3 Hz and waveforms longer than 200 μs were considered to be putative excitatory cells and included in analysis. DG cells with an average firing rate of less than 3 Hz and waveforms longer than 150 μs were considered to be putative DG granule or mossy cells.

DG cell firing properties

For each DG cell, average firing rates were calculated in (i) inner areas < 83 cm from the maze center and (ii) arm end areas > 83 cm from the maze center (Fig. 2b–e). The activity patterns of a cell were considered selective for inner areas, both areas, or arm end areas if the ratio of the average firing rate in inner area to the average firing rate in end area was > 150 %, 66.6–150 %, or < 66.6 %, respectively. A cell was defined as silent if the firing rate during the WM task was < 0.01 Hz. To quantify the spatial selectivity of DG cell firing, we created two $N \times 8$ arms matrices of firing rates, one for the inner segments and one for the arm ends. With each of the matrices, we conducted a repeated-measures ANOVA with factors arms and trials to measure arm selectivity. The ANOVAs were performed for each DG cell separately, and cells with $P < 0.05$ were considered as spatial.

CA3 place cell firing properties

Spatial firing-rate distributions for each well-isolated neuron were constructed by dividing the total number of spikes in each location bin (10×10 cm) by the amount of time that the animal spent in that location. Data were then smoothed by a two-dimensional convolution with a Gaussian kernel with a standard deviation of one pixel (10 cm), and the peak firing rate was the maximum firing rate in any of the pixels. In addition, the average firing rate was

calculated across all trials in the WM task, and cells with an average firing rate of < 0.05 Hz in behavior were excluded from further analysis. To describe place field properties, we calculated information per spike and sparsity of hippocampal place cells as previously described[54].

For spatial correlation analysis, firing patterns of individual cells were compared between trials[2,55]. For each cell, a separate spatial map was calculated for each trial, and the Pearson correlation coefficient between firing rates in corresponding pixels was calculated between all trial pairs. All pairwise correlation coefficients were then averaged. Spatial maps between the WM and the RF tasks were compared by first generating a spatial map averaged across all trials in the WM task and a spatial map for the entire 10-min recording session in the RF task, and by then calculating Pearson's correlation coefficient between the two maps.

Prospective ratio

Prospective firing was tested in CA3 cells that had place fields on select arms of the WM task. To determine arm-specific firing of each CA3 cell, average firing rates in individual arms (including the reward location) were calculated across all trials. For each cell, we then defined preferred arms as those in which the cell's firing rate in one arm was >0.5 Hz and at least 2.0 times higher than the firing rate averaged over all the other arms. If two preferred arms per cell were found, the arms with the higher and lower firing rates were defined as the primary and secondary preferred arm, respectively. Spikes that occurred during reward consumption before visiting the primary arm were defined as prospective spikes, and spikes that occurred during reward consumption after visiting the primary arm were defined as retrospective spikes. To not confound reward-related with spatial firing, both the primary and secondary arms were excluded from reward related calculations. Due to the limited sampling duration at reward locations within a single trial, we pooled prospective spikes and pooled retrospective spikes over all trials (10–20 trials) of a recording session and normalized by the total amount of time that the rat spent in reward periods. Note that the interaction between the sequence of arm visits and the location of the field did not bias our results as recordings included 10–20 trials in which the sequence of arm visits was randomized between trials. The likelihood that the visit to the arm with the place field occurred early or late in the trial was therefore counterbalanced. For each cell, we then calculated a prospective ratio (difference between prospective and retrospective firing rate divided by the sum of both rates)[15]. The ratio ranged between –1 and +1, with a positive value indicating a cell's bias toward representing future positions while the rat is at reward locations. In addition, the relative timing of firing compared to ripple generation was examined with cross-correlograms (10 ms bin size) between CA3 firing and reward-associated ripple events (Fig. 7c).

Postmortem histology

Electrodes were not moved after the final recording session. Rats received an overdose of sodium pentobarbital and were perfused intracardially with ~200 ml of 0.37 % sulphide solution (49 mM Na_2S, and 86 mM NaH_2PO_4, pH 7.2) or phosphate buffered saline (PBS) for 10 min, and 200 ml of 4 % paraformaldehyde in PBS (pH 7.4) for 10 min. To aid the reconstruction of electrode tracks, the electrodes were not withdrawn from the brain until 3–

4 hours after perfusion. Brains were then extracted, placed in 4 % paraformaldehyde overnight, and transferred to 30 % sucrose in phosphate buffered saline until equilibrated. Frozen coronal sections (40 μm) were cut using a microtome, and serial sections were mounted. Sections for 10 recording animals were stained with cresyl violet, sections from 11 dentate-lesioned recording animals were stained with Timm and cresyl violet and sections from the 16 animals with only behavioral testing were immunostained with NeuN. The cresyl violet stain was used to label all hippocampal cells with a counterstain in order to facilitate the verification of recording tetrode locations and the quantification of the dentate lesions (Fig. 2a, 3a). A NeuN immunostain was used to label all hippocampal neurons to quantify the dentate lesions in behavioral animals (Fig. 1c). The Timm stain was used to label mossy fiber (MF) projections from the dentate granule neurons to the CA3 pyramidal neurons in black[56,57], which was used in DG-lesioned rats to score any degree of remaining mossy fiber innervation within the CA3 stratum lucidum (Fig. 4b).

For combined cresyl violet and Timm staining, slide-mounted sections were first placed in a developer solution for ~75 min in darkness at room temperature[56, 57]. The developer solution consisted of 120 ml gum arabic solution (500 g gum arabic/l water), 60 ml hydroquinone solution (3.41 g hydroquinone), 10 ml citrate buffer (2.55 g citric acid, 2.06 g sodium citrate), and 1 ml silver nitrate solution (0.17 g silver nitrate). The slices were then rinsed in water and counterstained with cresyl violet. For NeuN immunostaining, immunoperoxidase procedures were performed on every sixth free floating section. After 1 hour of incubation in blocking solution (5% horse serum and 0.25% Triton X-100 in PBS) antibody incubations were done in PBS at room temperature overnight. The following antibodies were used: NeuN (mouse monoclonal; 1:15000; Millipore: MAB377) and biotinylated anti-mouse (1:1000; Vector Laboratories: BA-2000). The immune reaction was amplified by one hour incubation with an ABC kit (1:1000; Vector Laboratories: PK-6100) and developed with 3, 3′ diaminobenzidine substrate (DAB; 0.5 mg/ml; AMRESCO: E733) for 100 seconds. At the end of the staining procedures all the tissue was coverslipped using Permount (Fisher Scientific: SP15–500).

Three-dimensional reconstruction of the tetrode array

For histology from animals in electrophysiological recording experiments each section through segments of the hippocampus with electrode tracks was collected. All tetrodes of the 14-tetrode bundle were identified by matching tetrode positions in the bundle with electrode tracks in postmortem tissue[2,55]. Recordings from a tetrode were included in the data analysis if the tetrode's deepest position could be clearly assigned to either DG or CA3 (Fig. 2a, 3a and 4a, and Supplementary Fig. 2).

Quantification of DG lesion and mossy fiber score

The volume of the granule cell layer was measured in NeuN labelled and cresyl violet-positive sections throughout the entire dorsoventral extent of the DG with computer-based 3-D volumetry. Lesion accuracy and quality were quantified using the Cavalieri estimator application in the Stereo Investigator software (grid spacing of 20 μm, 10x objective) for volume quantification of the granule cell layer. The remaining granule cell volume of each DG-lesioned animal was normalized to a control volume of 430×10^7 μm^3 ($n = 5$ animals).

For measurements of lesions with cresyl violet-stained tissue, the estimate of the remaining DG granule cell volume can be expected to be an upper bound for the proportion of remaining granule cells because stained non-granule cells, such as glia, were also counted as remaining volume. CA3 and CA1 hippocampal subregions were also inspected in the DG-lesioned animals (Supplementary Fig. 1c).

For recording animals with DG lesions, any remaining granule cell innervation was quantified by examining the TIMM staining of MFs at CA3 recording sites. The distribution of Timm-positive signal at each tetrode tip in the CA3 striatum lucidum was scored according to the following criteria (Fig. 4b):

0   No Timm-positive staining (black reaction products). Signals comparable to background intensity in neighboring areas such as the CA3 stratum radiatum and stratum lacunosum moleculare.

1   Weak Timm-positive labeling. Less than 50 % of Timm-positive layer thickness and less than 30 % of Timm-positive signal intensity compared to control sections.

2   Moderate Timm-positive labeling was detected. More than 50 % of Timm-positive layer thickness, but less than 70 % of Timm-positive signal intensity compared to control sections.

3   Abundant Timm-positive labeling was detected. More than 50 % of Timm-positive layer thickness and more than 70 % of Timm-positive signal intensity compared to control slices.

4   Control (no DG lesion).

The scores above were combined into two groups: scores of 0 and 1 were classified as the low-density MF group (lMF), and scores of 2 were classified as the high-density MF group (hMF). No tetrodes in lesioned rats received a score of 3.

For analysis by CA3 subregions, we defined CA3c as the area of the CA3 pyramidal cell layer between the two blades of the dentate granule cell layer. The remaining area of the CA3 pyramidal cell layer was defined as CA3a,b. In control animals, 8 and 9 tetrodes were located at CA3a,b and CA3c, respectively. In DG-lesioned animals, 12 and 12 tetrodes were located at CA3a,b and CA3c, respectively.

Statistical Analysis

Unless specified otherwise, both correct and incorrect trials were included in all reported analyses. If incorrect trials were included, only the first entry into the arm (i.e., when reward was present) was included in the analysis. All data are presented as mean ± standard error of the mean (SEM) and were analyzed using Matlab. Two-sample comparisons were performed by two-sided *t* test or, if the data did not meet the assumptions of the *t* test, were analyzed with the nonparametric two-sided Mann-Whitney U-test. Multiple group comparisons of normalized ripple rates were assessed using a repeated-measures ANOVA, followed by Scheffé test when necessary. Multiple group comparisons of mean firing properties were performed by Mann-Whitney U-test followed by posthoc Bonferroni corrections. The null

hypothesis was rejected at the $P < 0.05$ level. No statistical methods were used to pre-determine sample sizes but our sample sizes are similar to those reported in previous publications[58]. Data collection and analysis were not performed blind to the conditions of the experiments.

Data Availability

The data that support the findings of this study are available from the corresponding author upon reasonable request.

Code Availability

The code that support the findings of this study are available from the corresponding author upon reasonable request.

Supplementary Material

Refer to Web version on PubMed Central for supplementary material.

Acknowledgments

References

1. Xavier GF, Costa VC. Dentate gyrus and spatial behaviour. Prog Neuropsychopharmacol Biol Psychiatry. 2009; 33:762–773. [PubMed: 19375476]

2. Leutgeb JK, Leutgeb S, Moser MB, Moser EI. Pattern separation in the dentate gyrus and CA3 of the hippocampus. Science. 2007; 315:961–966. [PubMed: 17303747]

3. Neunuebel JP, Knierim JJ. CA3 retrieves coherent representations from degraded input: direct evidence for CA3 pattern completion and dentate gyrus pattern separation. Neuron. 2014; 81:416–427. [PubMed: 24462102]

4. Amaral DG, Witter MP. The three-dimensional organization of the hippocampal formation: a review of anatomical data. Neuroscience. 1989; 31:571–591. [PubMed: 2687721]

5. Scharfman HE. The CA3 "backprojection" to the dentate gyrus. Progress in brain research. 2007; 163:627–637. [PubMed: 17765742]

6. Treves A, Rolls ET. Computational analysis of the role of the hippocampus in memory. Hippocampus. 1994; 4:374–391. [PubMed: 7842058]

7. Lisman JE, Talamini LM, Raffone A. Recall of memory sequences by interaction of the dentate and CA3: a revised model of the phase precession. Neural networks: the official journal of the International Neural Network Society. 2005; 18:1191–1201. [PubMed: 16233972]

8. Buzsaki G. Hippocampal sharp waves: their origin and significance. Brain research. 1986; 398:242–252. [PubMed: 3026567]

9. Csicsvari J, Hirase H, Mamiya A, Buzsaki G. Ensemble patterns of hippocampal CA3-CA1 neurons during sharp wave-associated population events. Neuron. 2000; 28:585–594. [PubMed: 11144366]

10. Oliva A, Fernandez-Ruiz A, Buzsaki G, Berenyi A. Role of Hippocampal CA2 Region in Triggering Sharp-Wave Ripples. Neuron. 2016; 91:1342–1355. [PubMed: 27593179]

11. Buzsaki G, Horvath Z, Urioste R, Hetke J, Wise K. High-frequency network oscillation in the hippocampus. Science. 1992; 256:1025–1027. [PubMed: 1589772]

12. Lee AK, Wilson MA. Memory of sequential experience in the hippocampus during slow wave sleep. Neuron. 2002; 36:1183–1194. [PubMed: 12495631]

13. Foster DJ, Wilson MA. Reverse replay of behavioural sequences in hippocampal place cells during the awake state. Nature. 2006; 440:680–683. [PubMed: 16474382]

14. Pfeiffer BE, Foster DJ. Hippocampal place-cell sequences depict future paths to remembered goals. Nature. 2013; 497:74–79. [PubMed: 23594744]

15. Diba K, Buzsaki G. Forward and reverse hippocampal place-cell sequences during ripples. Nature neuroscience. 2007; 10:1241–1242. [PubMed: 17828259]

16. Karlsson MP, Frank LM. Awake replay of remote experiences in the hippocampus. Nature neuroscience. 2009; 12:913–918. [PubMed: 19525943]

17. Carr MF, Jadhav SP, Frank LM. Hippocampal replay in the awake state: a potential substrate for memory consolidation and retrieval. Nature neuroscience. 2011; 14:147–153. [PubMed: 21270783]

18. Dupret D, O'Neill J, Pleydell-Bouverie B, Csicsvari J. The reorganization and reactivation of hippocampal maps predict spatial memory performance. Nature neuroscience. 2010; 13:995–1002. [PubMed: 20639874]

19. Ego-Stengel V, Wilson MA. Disruption of ripple-associated hippocampal activity during rest impairs spatial learning in the rat. Hippocampus. 2010; 20:1–10. [PubMed: 19816984]

20. Girardeau G, Benchenane K, Wiener SI, Buzsaki G, Zugaro MB. Selective suppression of hippocampal ripples impairs spatial memory. Nature neuroscience. 2009; 12:1222–1223. [PubMed: 19749750]

21. Jadhav SP, Kemere C, German PW, Frank LM. Awake hippocampal sharp-wave ripples support spatial memory. Science. 2012; 336:1454–1458. [PubMed: 22555434]

22. Sullivan D, et al. Relationships between hippocampal sharp waves, ripples, and fast gamma oscillation: influence of dentate and entorhinal cortical activity. The Journal of neuroscience: the official journal of the Society for Neuroscience. 2011; 31:8605–8616. [PubMed: 21653864]

23. Penttonen M, Kamondi A, Sik A, Acsady L, Buzsaki G. Feed-forward and feed-back activation of the dentate gyrus in vivo during dentate spikes and sharp wave bursts. Hippocampus. 1997; 7:437–450. [PubMed: 9287083]

24. Bragin A, Jando G, Nadasdy Z, van Landeghem M, Buzsaki G. Dentate EEG spikes and associated interneuronal population bursts in the hippocampal hilar region of the rat. Journal of neurophysiology. 1995; 73:1691–1705. [PubMed: 7643175]

25. Senzai Y, Buzsaki G. Physiological Properties and Behavioral Correlates of Hippocampal Granule Cells and Mossy Cells. Neuron. 2017; 93:691–704e695. [PubMed: 28132824]

26. Danielson NB, et al. In Vivo Imaging of Dentate Gyrus Mossy Cells in Behaving Mice. Neuron. 2017; 93:552–559e554. [PubMed: 28132825]

27. GoodSmith D, et al. Spatial Representations of Granule Cells and Mossy Cells of the Dentate Gyrus. Neuron. 2017; 93:677–690e675. [PubMed: 28132828]

28. O'Neill J, Senior T, Csicsvari J. Place-selective firing of CA1 pyramidal cells during sharp wave/ripple network patterns in exploratory behavior. Neuron. 2006; 49:143–155. [PubMed: 16387646]

29. Buzsaki G. Hippocampal sharp wave-ripple: A cognitive biomarker for episodic memory and planning. Hippocampus. 2015; 25:1073–1188. [PubMed: 26135716]

30. Kay K, et al. A hippocampal network for spatial coding during immobility and sleep. Nature. 2016; 531:185–190. [PubMed: 26934224]

31. Ahmed OJ, Mehta MR. Running speed alters the frequency of hippocampal gamma oscillations. The Journal of neuroscience: the official journal of the Society for Neuroscience. 2012; 32:7373–7383. [PubMed: 22623683]

32. Leutgeb S, Leutgeb JK. Pattern separation, pattern completion, and new neuronal codes within a continuous CA3 map. Learn Mem. 2007; 14:745–757. [PubMed: 18007018]

33. Singer AC, Carr MF, Karlsson MP, Frank LM. Hippocampal SWR activity predicts correct decisions during the initial learning of an alternation task. Neuron. 2013; 77:1163–1173. [PubMed: 23522050]

34. McLamb RL, Mundy WR, Tilson HA. Intradentate colchicine disrupts the acquisition and performance of a working memory task in the radial arm maze. Neurotoxicology. 1988; 9:521–528. [PubMed: 3200514]

35. Jung MW, McNaughton BL. Spatial selectivity of unit activity in the hippocampal granular layer. Hippocampus. 1993; 3:165–182.

36. Neunuebel JP, Knierim JJ. Spatial firing correlates of physiologically distinct cell types of the rat dentate gyrus. The Journal of neuroscience: the official journal of the Society for Neuroscience. 2012; 32:3848–3858. [PubMed: 22423105]

37. Myers CE, Scharfman HE. Pattern separation in the dentate gyrus: a role for the CA3 backprojection. Hippocampus. 2011; 21:1190–1215. [PubMed: 20683841]

38. Colgin LL. Do slow and fast gamma rhythms correspond to distinct functional states in the hippocampal network? Brain research. 2015; 1621:309–315. [PubMed: 25591484]

39. Atallah BV, Scanziani M. Instantaneous modulation of gamma oscillation frequency by balancing excitation with inhibition. Neuron. 2009; 62:566–577. [PubMed: 19477157]

40. Tort AB, Komorowski RW, Manns JR, Kopell NJ, Eichenbaum H. Theta-gamma coupling increases during the learning of item-context associations. Proceedings of the National Academy of Sciences of the United States of America. 2009; 106:20942–20947. [PubMed: 19934062]

41. Carr MF, Karlsson MP, Frank LM. Transient slow gamma synchrony underlies hippocampal memory replay. Neuron. 2012; 75:700–713. [PubMed: 22920260]

42. Hsiao YT, Zheng C, Colgin LL. Slow gamma rhythms in CA3 are entrained by slow gamma activity in the dentate gyrus. Journal of neurophysiology. 2016; 116:2594–2603. [PubMed: 27628206]

43. Igarashi KM, Lu L, Colgin LL, Moser MB, Moser EI. Coordination of entorhinal-hippocampal ensemble activity during associative learning. Nature. 2014; 510:143–147. [PubMed: 24739966]

44. Martin C, Beshel J, Kay LM. An olfacto-hippocampal network is dynamically involved in odor-discrimination learning. Journal of neurophysiology. 2007; 98:2196–2205. [PubMed: 17699692]

45. Rangel LM, Chiba AA, Quinn LK. Theta and beta oscillatory dynamics in the dentate gyrus reveal a shift in network processing state during cue encounters. Frontiers in systems neuroscience. 2015; 9:96. [PubMed: 26190979]

46. McNaughton BL, Barnes CA, Meltzer J, Sutherland RJ. Hippocampal granule cells are necessary for normal spatial learning but not for spatially-selective pyramidal cell discharge. Experimental brain research. 1989; 76:485–496. [PubMed: 2792242]

47. Hofer KT, et al. The hippocampal CA3 region can generate two distinct types of sharp wave-ripple complexes, in vitro. Hippocampus. 2015; 25:169–186. [PubMed: 25209976]

48. Pfeiffer BE, Foster DJ. Autoassociative dynamics in the generation of sequences of hippocampal place cells. Science. 2015; 349:180–183. [PubMed: 26160946]

49. Walsh TJ, Schulz DW, Tilson HA, Schmechel DE. Colchicine-induced granule cell loss in rat hippocampus: selective behavioral and histological alterations. Brain research. 1986; 398:23–36. [PubMed: 3801898]

50. Goldschmidt RB, Steward O. Preferential neurotoxicity of colchicine for granule cells of the dentate gyrus of the adult rat. Proceedings of the National Academy of Sciences of the United States of America. 1980; 77:3047–3051. [PubMed: 6930683]

51. Goldschmidt RB, Steward O. Neurotoxic effects of colchicine: differential susceptibility of CNS neuronal populations. Neuroscience. 1982; 7:695–714. [PubMed: 7070670]

52. Brandon MP, Koenig J, Leutgeb JK, Leutgeb S. New and distinct hippocampal place codes are generated in a new environment during septal inactivation. Neuron. 2014; 82:789–796. [PubMed: 24853939]

53. Redish, AD. MClust 3.5, Free-Ware Spike Sorting. University of Minnesota; Minneapolis: 2009. Available at http://redishlab.neuroscience.umn.edu/MClust/MClust.html

54. Skaggs WE, McNaughton BL, Wilson MA, Barnes CA. Theta phase precession in hippocampal neuronal populations and the compression of temporal sequences. Hippocampus. 1996; 6:149–172. [PubMed: 8797016]

55. Koenig J, Linder AN, Leutgeb JK, Leutgeb S. The spatial periodicity of grid cells is not sustained during reduced theta oscillations. Science. 2011; 332:592–595. [PubMed: 21527713]

56. Cavazos JE, Golarai G, Sutula TP. Mossy fiber synaptic reorganization induced by kindling: time course of development, progression, and permanence. The Journal of neuroscience: the official journal of the Society for Neuroscience. 1991; 11:2795–2803. [PubMed: 1880549]

57. Buckmaster PS, Dudek FE. Network properties of the dentate gyrus in epileptic rats with hilar neuron loss and granule cell axon reorganization. Journal of neurophysiology. 1997; 77:2685–2696. [PubMed: 9163384]

58. Schlesiger MI, et al. The medial entorhinal cortex is necessary for temporal organization of hippocampal neuronal activity. Nature neuroscience. 2015; 18:1123–1132. [PubMed: 26120964]
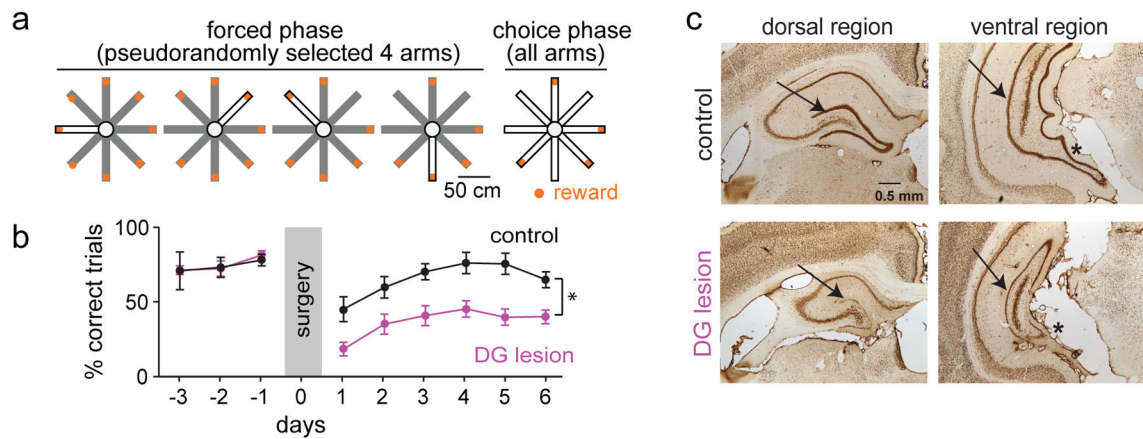
Figure 1. Selective dentate granule cell lesions impaired spatial working memory
(**a**) A spatial working memory (WM) task was performed on an 8-arm radial maze with reward locations (orange) at the end of each arm. Four arms were individually presented during the forced phase, after which all arms were made available in the choice phase. Open and closed arms in the schematic are shown in white and gray, respectively. (**b**) Mean (± SEM) percent correct performance in the spatial WM task as a function of testing days. Selective pharmacological lesions of dentate granule neurons with colchicine resulted in significant memory impairment ($n = 5$ control rats, 11 lesioned rats; $F(1,70) = 16.07$, $P = 0.0013$, repeated-measures ANOVA). * $P < 0.05$, comparison between groups. (**c**) Coronal brain sections of the dorsal and ventral hippocampus labelled with NeuN in a control rat (top) and a DG-lesioned rat (bottom). Sections from control and DG-lesioned rats are at the same coordinate from bregma. Arrows point to the dentate granule cell layer. Asterisks highlight the reduction in ventral DG volume in the lesion compared to control rat.
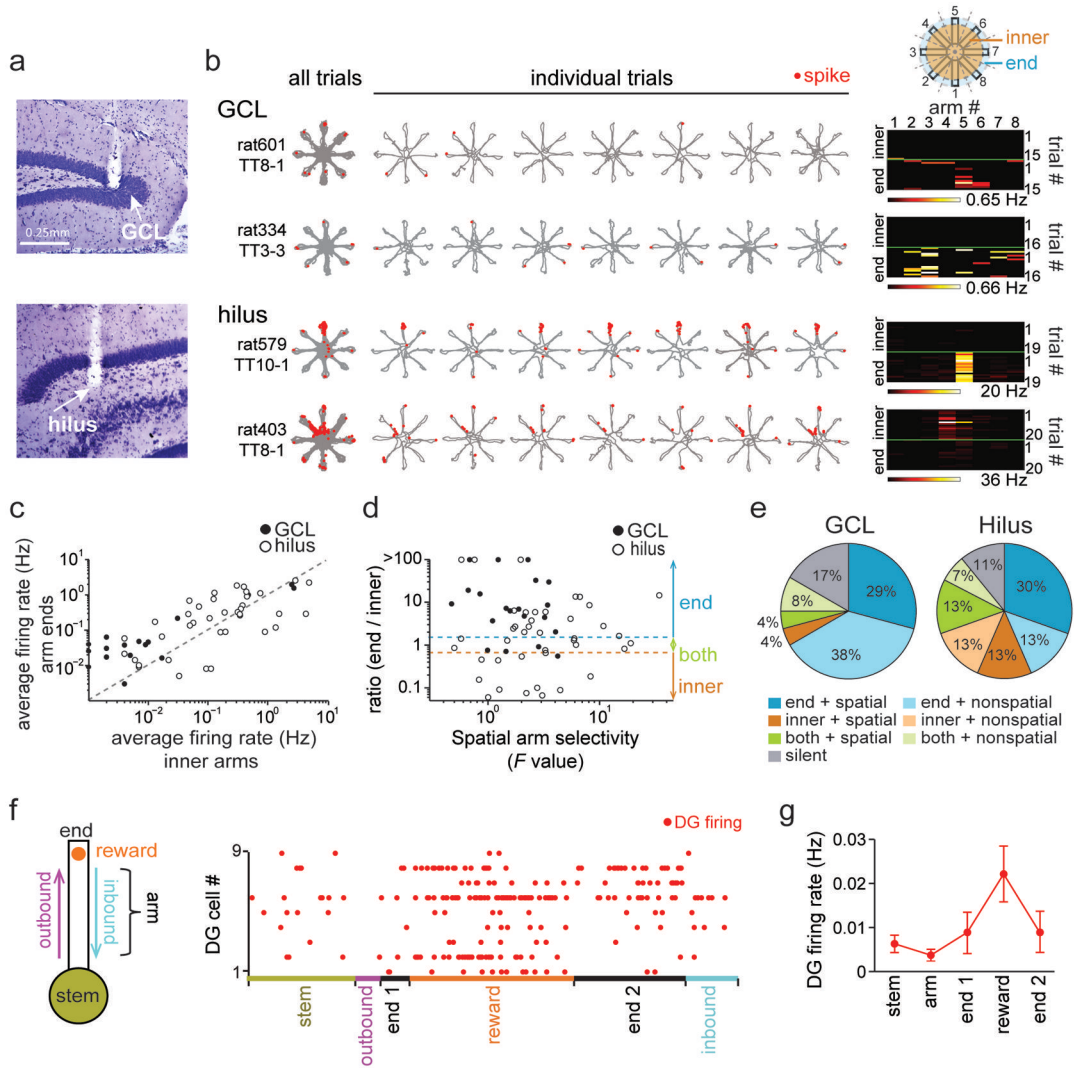
Figure 2. Reward-selective firing of dentate cells
(**a**) Histological confirmation of recording sites (white arrows) in the DG granule cell layer (GCL, top) and the hilus (bottom) in a cresyl-stained section. (**b**) Representative firing patterns of cells recorded from the GCL and hilus in the spatial WM task. Similar results were obtained in 24 GCL and 47 hilus cells from 4 control rats and are quantified in panels (c–e). Each row is the activity pattern of a single dentate neuron. The trajectories (gray) with spike locations (red dots) are shown superimposed for all trials in a recording session and separately for the first 7 of up to 20 trials (from left to right). (Rightmost) Color coded matrix that summarizes the firing pattern of the cell example over the entire spatial WM session. Firing rate is represented by a color scale from zero (black) to the highest peak in the session (white, corresponding to the number at the bottom of the matrix). The top half of the matrix corresponds to the firing rates on the arms ('inner') and the bottom half to the firing on the arm ends ('end'). Note that two distinct types of firing patterns are evident in these matrices, either location-selective firing across trials (hilus, rat579, TT10-1; hilus, rat403, TT8-1) or selective firing at a subset of reward locations (GCL, rat601, TT8-1; GCL,

rat334, TT3-3). (**c**) Average firing rates of dentate cells on the maze arms compared to the arm ends ($n = 24$ GCL cells, filled circles; and 47 hilus cells, open circles). Each dot is a single dentate cell. (**d**) The ratio of the firing rate at the arm ends compared to the maze arms is plotted against a statistical measure of arm selectivity (F value from an ANOVA with rate by arm and trials as factors). Dotted blue and orange lines represent ratios of 3/2 and 2/3, respectively, which correspond to the cutoffs for selectivity to arm ends and inner arms. Cells with ratios in-between were considered active in both segments. (**e**) Proportion of dentate neurons classified based on the plot in (d). Cells with an average firing rate < 0.01 Hz on the maze were defined as silent cells. Cells with *P* values < 0.05 in the ANOVA were defined as spatial cells. (**f**) Firing of example dentate cells during distinct periods within each trial. Periods were defined and colored coded as indicated in the schematic on the left, and the arm end was divided into the time before, during, and after reward consumption (arm end 1, reward, and arm end 2, respectively). The length of each behavioral period in the illustration corresponds to its average duration in a trial. (**g**) Average frequency (± SEM) of behavior-related DG cell spikes ($n = 16$ cells). Increased firing occurred during reward consumption.
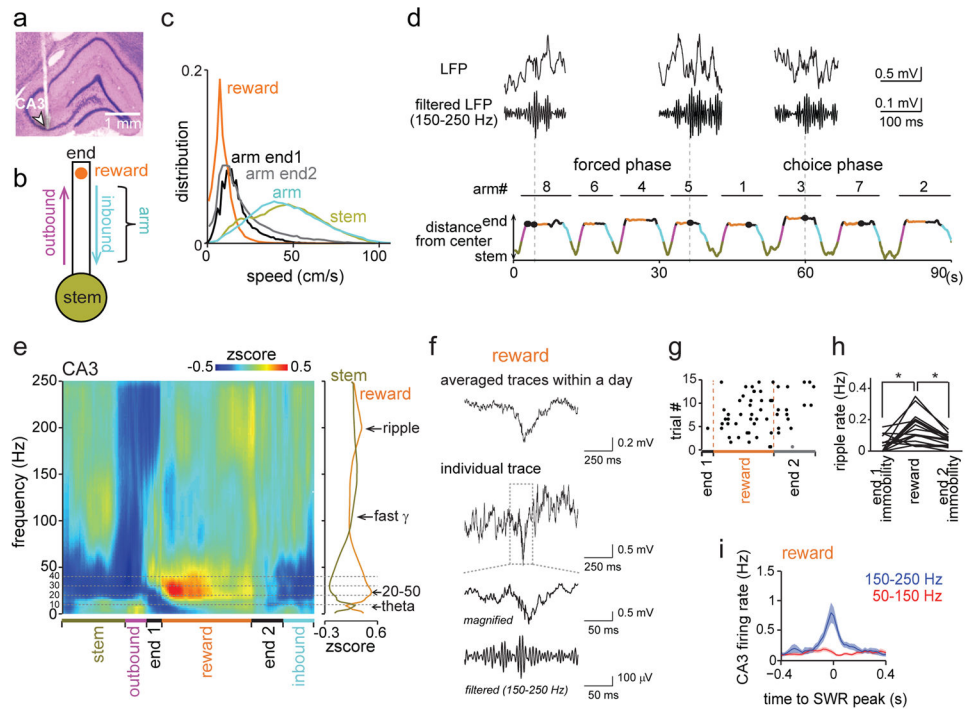
Figure 3. CA3 ripple events during the spatial WM task

(**a**) Histological confirmation of a CA3 recording site (indicated by arrow). (**b**) Schematic of behavioral periods. (**c**) Running speed distribution for the periods defined in (b). Data from 4 control rats with reward sensors were combined. Immobility and low running speeds were only observed on arm ends (before, during, and after reward consumption). (**d**) SWR events at arm ends plotted by time within the trial and distance from the center of the maze. Behavioral periods are colored as in (b). Unfiltered and bandpass-filtered (150–250 Hz) LFP traces of example high-frequency events are shown on top. Vertical stippled lines indicate correspondence to the time line. (**e**) (Left) LFP power spectrogram from a CA3 recording site. Trials from one recording day were averaged. Progression through behavioral periods is indicated at the bottom. (Right) Average LFP power during reward and stem periods as a function of frequency (n = 18 trials, 8 reward periods per trial). The peak frequency was in the 20–50 Hz range and in the 150–250 Hz range during reward consumption and in the theta range at the stem. See Supplementary Fig. 7a–c for related analyses. (**f**) Averages of all SWR events in the session (top; n = 111 events) and an individual event at different time scales (Supplementary Fig. 8a for additional examples from other animals and the average over all animals). (**g**) Occurrence of SWRs in all trials of a recording day. For visualization of the distribution over multiple trials, each behavioral period within a trial was normalized to the average length of the corresponding period. CA3 SWRs primarily occurred during reward consumption. (**h**) Comparison of SWR rates between periods of reward consumption and immobility at arm ends (*n* = 17 tetrodes from 4 animals, reward vs periods of end immobility, F(2,48) = 13.07, *P* = 2.9 × 10^{-5}, ANOVA, *P* < 0.01, Scheffé test). Each line represents a CA3 recording site. * *P* < 0.05. (**i**) Event-triggered firing rate (mean ± SEM for each 20 ms bins) for CA3 pyramidal cells (*n* = 116 from 17 tetrodes in 4 animals). LFP signals were band-pass filtered in two separate frequency bands (50–150 Hz and 150–250
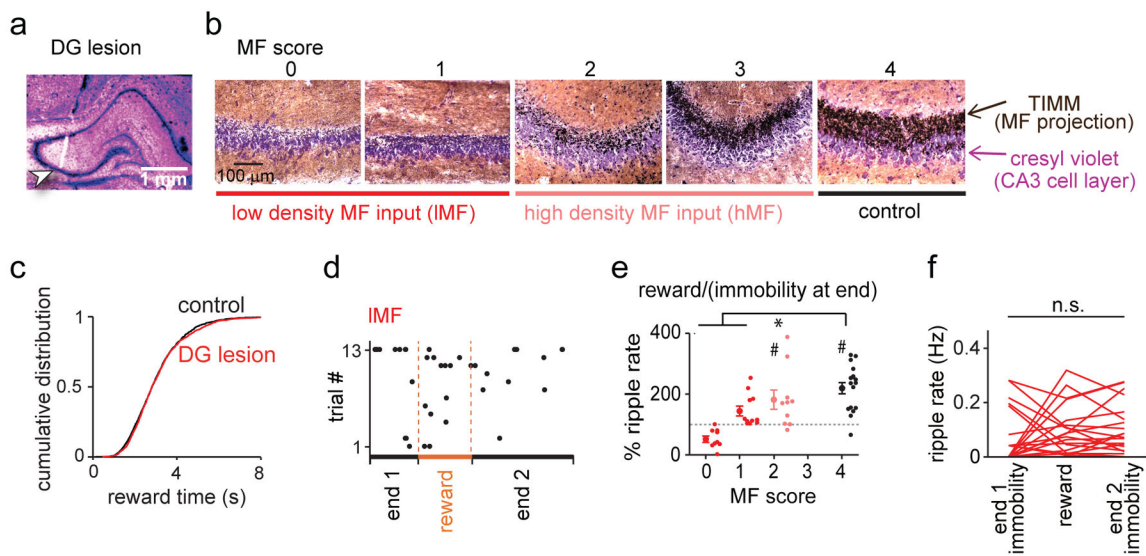
Hz), and events detected when the root mean-square power of the filtered traces exceeded 3 standard deviations (SDs) above the mean.

Figure 4. Reward-associated CA3 SWR events were dependent on direct mossy fiber input from the dentate gyrus

(**a**) Histological confirmation of a CA3 recording site in a DG-lesioned rat (indicated by arrow). (**b**) Mossy fiber (MF) density was scored at each recording site in the hippocampal CA3 subregion on a scale from 0 (no MF input) to 4 (control MF input). Scores 0–1 were combined into the low-density MF input (lMF) group and higher scores were considered high-density MF input (hMF) group. Cell bodies are labelled with cresyl violet (purple), and MF of dentate granule cells are labelled with TIMM (black). (**c**) Cumulative distribution of duration of reward intake ($n = 1521$ and 1585 in control and lesioned rats, respectively; $D_{max} = 0.032$, $P = 0.42$, Kolmogorov-Smirnov test). (**d**) Same as Fig. 3g but for a lMF CA3 recording site in a DG-lesioned animal. (**e**) Percent ripple event rates during reward compared to periods of immobility on arm ends for each CA3 recording site (dots represent individual CA3 recording sites, grouped by the MF score) (score 0: n = 9 from 6 animals, $t(8) = 0.24$, $P = 0.81$; score 1: n = 11 from 6 animals, $t(10) = 0.72$, $P = 0.49$; score 2: n = 10 from 5 animals, $t(9) = 2.71$, $P = 0.024$; score 4: n = 17 from 4 animals, $t(16) = 4.99$, $P = 1.3 \times 10^{-4}$, two-sided paired *t* test within the group; control vs lMF, U = 211, Z = 3.71, $P = 2.0 \times 10^{-4}$; control vs hMF, U = 116, Z = 1.18, $P = 0.24$, two-sided Mann-Whitney U test followed by posthoc Bonferroni corrections). The choice and forced phases are combined (see Supplementary Fig. 9 for additional related analyses). * $P < 0.05$, comparison across groups; # $P < 0.05$, reward vs immobility at end within group. (**f**) For the lMF group, ripple rates did not increase during reward compared to other immobile periods at arm ends ($n = 20$ tetrodes from 9 DG-lesioned animals; $F(2,57) = 0.67$, $P = 0.52$, ANOVA).
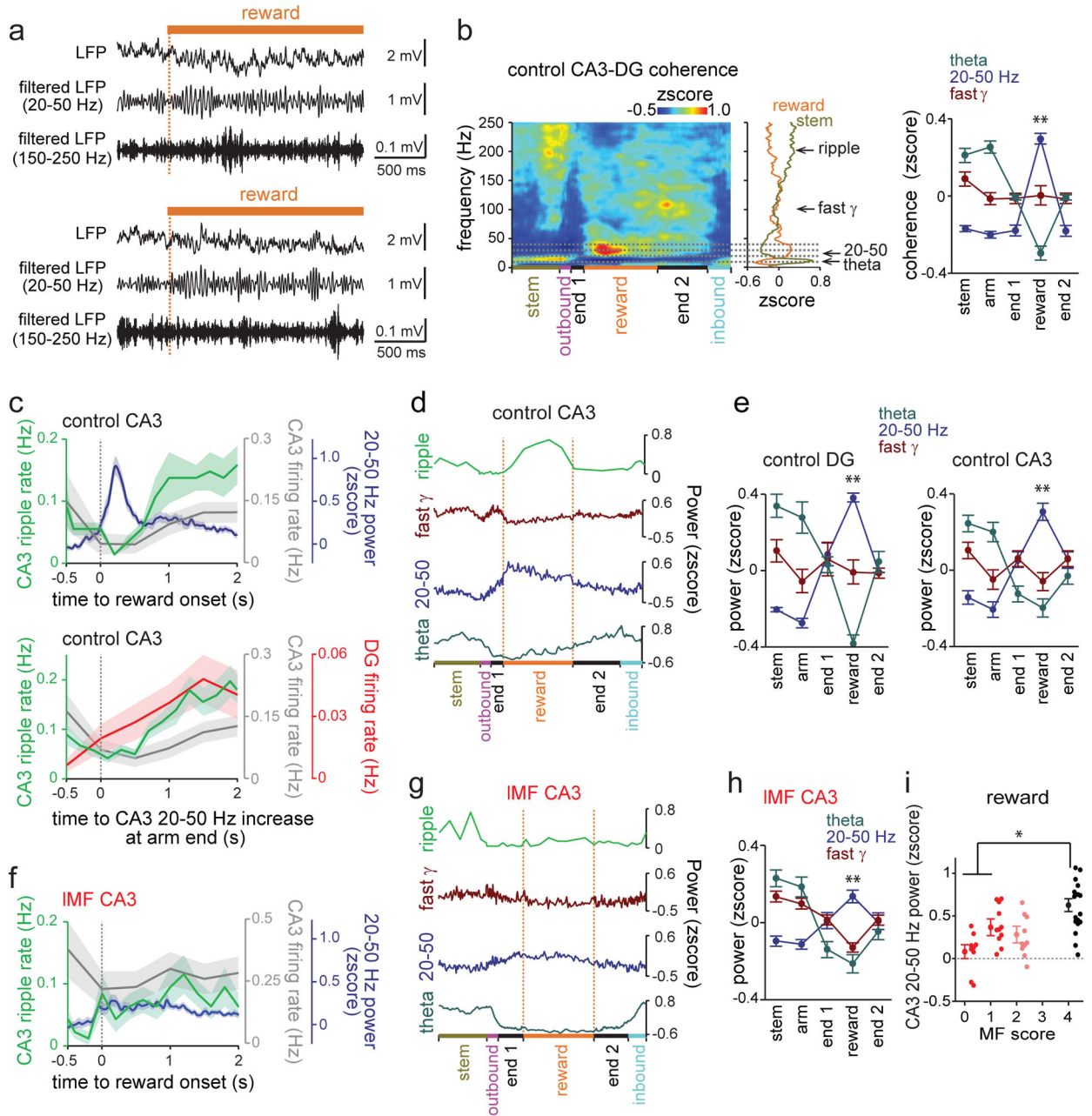
Figure 5. CA3 oscillations and DG-CA3 coherence in the 20–50 Hz range during reward consumption were dependent on MF input from DG to CA3

(**a**) Two typical unfiltered and bandpass-filtered (20–50 Hz and 150–250 Hz) LFP traces aligned to the onset of reward consumption (dashed line). (**b**) DG-CA3 LFP coherence in a control animal. The average across all trials within a recording day is shown. DG-CA3 coherence in the 20–50 Hz range increased during reward, as indicated by asterisks, and coherence in the theta range decreased during reward compared to stem and arm ($n = 35$ tetrode pairs from 4 control animals; theta: $F_{(4,136)} = 64.4$, $P < 10^{-10}$, 20–50 Hz: $F_{(4,136)} = 307.5$, $P < 10^{-10}$, fast gamma: $F_{(4,136)} = 8.7$, $P < 10^{-10}$, repeated measures ANOVAs, increase at reward vs all the other periods, ** $P < 0.01$, Scheffé test). (**c**) Time course of

reward-related LFP and single-unit activity in DG and CA3. (Top) CA3 ripple events (green, $n = 17$ tetrodes from 4 animals), CA3 20–50 Hz power (blue, $n = 17$ tetrodes from 4 animals), and firing rate of CA3 cells (gray, $n = 116$ cells from 4 animals) are aligned to the onset of reward consumption. At reward onset, 20–50 Hz activity increased whereas ripple event rate and CA3 firing rate was lowest. (Bottom) CA3 ripple events (green, $n = 17$ tetrodes from 4 animals) and firing rate of CA3 cells (gray, $n = 116$ from 4 animals) and dentate cells (red, $n = 16$ from 2 animals) are aligned to the onset of the increase in CA3 20–50 Hz power. Shaded areas are SEM. (**d**) Behavior-related CA3 ripple event rates and CA3 LFP power in the theta, 20–50 Hz, and fast gamma bands across different behavioral periods. (**e**) Average LFP power at individual frequency bands in control DG recordings ($n = 8$ tetrodes from 3 animals) and CA3 recordings ($n = 17$ tetrodes from 4 animals). 20–50 Hz power in DG and CA3 was increased while theta power was decreased during reward consumption (DG: theta: $F(4,28) = 26.6$, $P < 10^{-10}$, 20–50 Hz: $F(4,28) = 56.6$, $P < 10^{-10}$, fast gamma: $F(4,28) = 1.1$, $P = 0.38$; CA3: theta: $F(4,64) = 13.1$, $P < 10^{-10}$, 20–50 Hz: $F(4,64) = 22.7$, $P < 10^{-10}$, fast gamma: $F(4,64) = 2.4$, $P = 0.062$, repeated measures ANOVAs; increase at reward vs all the other periods, ** $P < 0.01$, Scheffé test). (**f**) Same as (c, top) but for lMF group (ripple events and 20–50 Hz power, $n = 20$ tetrodes from 9 animals; firing rate of CA3 cells, $n = 57$ cells from 9 animals). (**g**) Same as (d) but for lMF group. (**h**) Same as (e, right) but for lMF group ($n = 20$ tetrodes from 9 animals; theta: $F(4,76) = 29.5$, $P < 10^{-10}$, 20–50 Hz: $F(4,76) = 20.5$, $P < 10^{-10}$, fast gamma: $F(4,76) = 30.3$, $P < 10^{-10}$, repeated measures ANOVAs; increase at reward vs all the other periods, ** $P < 0.01$, Scheffé test). Error bars are SEM. (**i**) CA3 20–50 Hz power for CA3 recording sites (mean ± SEM, dots correspond to individual sites, grouped by the MF score). Reward-associated 20–50 Hz power was significantly reduced at CA3 sites with reduced MF input compared to control CA3 sites ($n = 9$, 11, 10, and 17 from 6, 6, 5, and 4 animals for score 0, 1, 2, and 4, respectively; control vs hMF, U = 288, Z = 2.49, $P = 0.26$; control vs lMF, U = 431, Z = 3.28, $P = 2.0 \times 10^{-4}$, two-sided Mann-Whitney U test followed by posthoc Bonferroni corrections). * $P < 0.05$, comparison across the groups. Error bars are SEM.
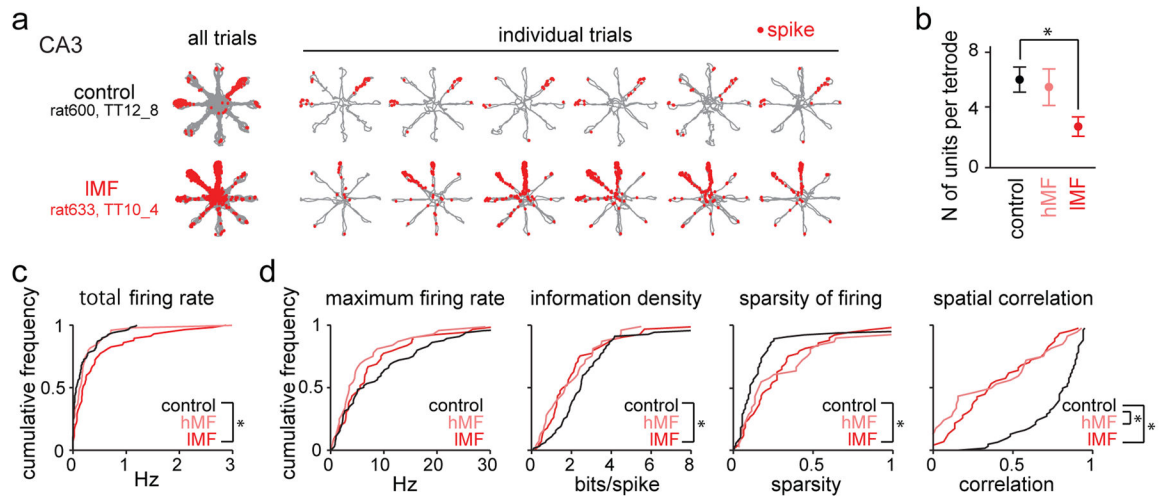
Figure 6. Place-specific firing of CA3 pyramidal neurons

(**a**) Each row is a representative example of place-specific firing of a CA3 pyramidal cell (top, control; bottom, DG-lesion) in the spatial WM task. Similar results were obtained in 116 control cells from 4 animals and in 57 lMF cells from 9 DG-lesioned rats and are quantified in panels (c) and (d). For each neuron, the trajectories (gray) with spike locations (red dots) are shown superimposed for all 20 trials in a recording session and separately for the first 6 trials (from left the right). CA3 place fields in control animals were frequently restricted to a single arm, but firing fields were broader at recording sites of DG-lesioned rats (see Supplementary Fig. 14 for additional examples). (**b**) Average number of CA3 principal cells that were recorded from each tetrode. Fewer CA3 neurons were detected at lMF sites, compared to CA3 recording sites from control rats and hMF sites from DG-lesioned rats ($n = 17$, 10, and 20 in control, hMF, lMF sites in 4, 5, and 9 animals, respectively; control vs hMF, $U = 250.5$, $Z = 0.61$, $P > 0.99$; control vs lMF, $U = 443.5$, $Z = 3.70$, $P = 4.2 \times 10^{-4}$, two-sided Mann-Whitney U test followed by posthoc Bonferroni corrections). * $P < 0.05$. Error bars are SEM. (**c**) Cumulative distribution of total firing rates for the entire sample of CA3 cells ($n = 116$, 48, and 57 cells from 4, 5, and 9 animals in control, hMF, and lMF groups, respectively). The firing rates of CA3 neurons were selectively increased at sites with low density MF input (lMF) (control vs hMF, $D_{max} = 0.20$, $P = 0.11$; control vs lMF, $D_{max} = 0.30$, $P = 0.0024$, Kolmogorov-Smirnov test with Bonferroni's correction). * $P < 0.05$. (**d**) Cumulative distribution of maximum in-field firing rates, information density scores, sparsity of firing, and spatial correlation for CA3 cells recorded from control, hMF, and lMF sites ($n = 64$, 34, and 47 cells from 4, 5, and 9 animals, respectively). Spatial measurements were calculated from all cells with an average firing rate > 0.05 Hz. The precision of spatial firing was reduced in DG-lesioned rats, and the effect was more pronounced at lMF sites (maximum firing rate, control vs hMF, $D_{max} = 0.26$, $P = 0.16$; control vs lMF, $D_{max} = 0.16$, $P = 0.84$; information density, control vs hMF, $D_{max} = 0.26$, $P = 0.15$; control vs lMF, $D_{max} = 0.30$, $P = 0.022$; sparsity, control vs hMF, $D_{max} = 0.30$, $P = 0.051$; control vs lMF, $D_{max} = 0.35$, $P = 0.0030$). However, reliability of spatial firing was reduced irrespective of MF density (spatial correlation, control vs hMF, $D_{max} = 0.56$, $P = 3.2 \times 10^{-6}$; control vs lMF, $D_{max} = 0.55$, *$P = 1.4 \times 10^{-7}$, Kolmogorov-Smirnov test with Bonferroni's correction). * $P < 0.05$.
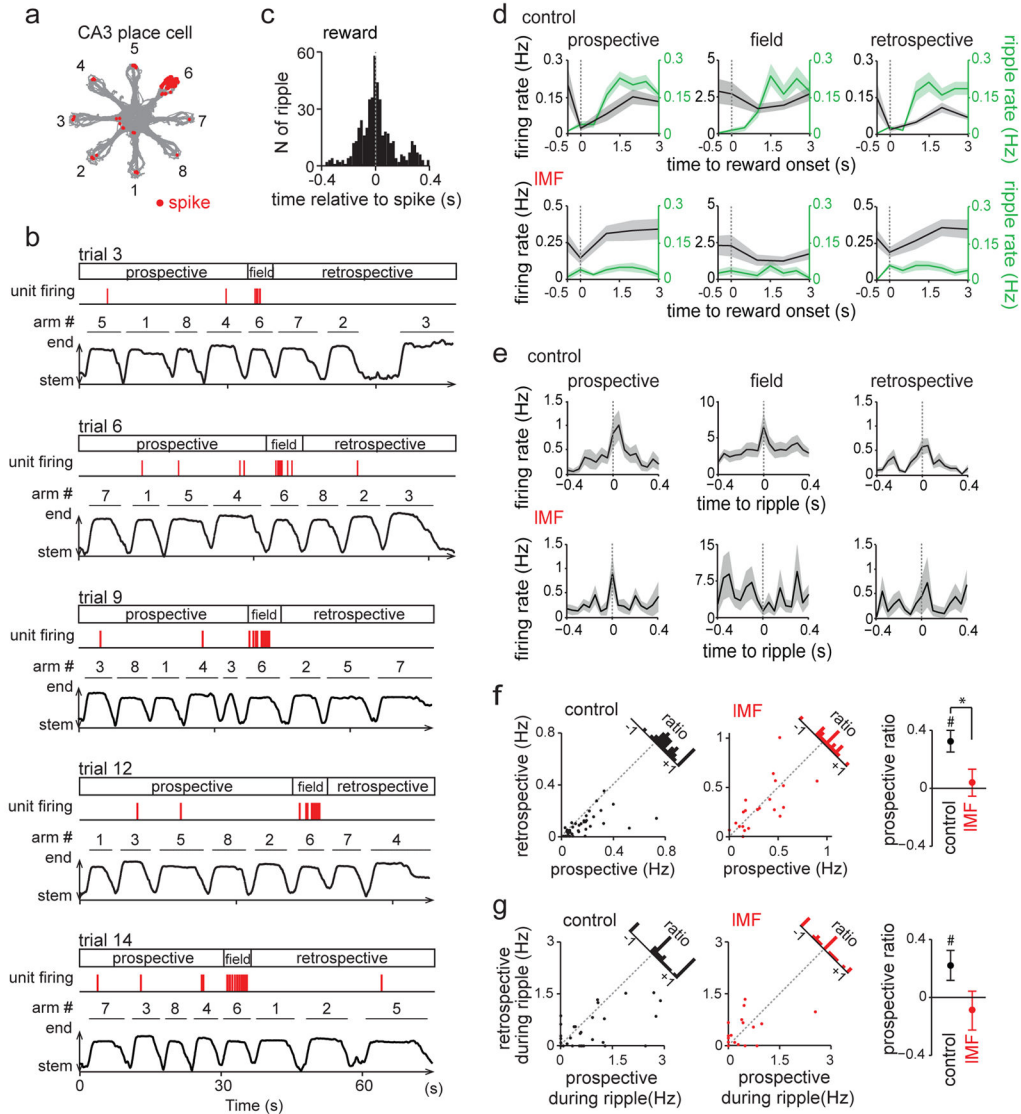
Figure 7. Prospective firing of CA3 neurons during sharp-wave ripples was dependent on direct MF innervation from the DG

(**a**) Spatial firing pattern of a representative CA3 neuron. Trajectories (gray) with spike locations (red dots) are superimposed for 20 trials of the WM task. The firing of the CA3 neuron was highest within the place field on arm 6 but spiking also occurred during ripples at reward locations. Similar place fields in predominantly one maze arm were found and analyzed for 39 control CA3 cells from 4 animals and 22 cells at lMF sites in 6 DG-lesioned animals. (**b**) Example trials show spiking within the field and at reward locations for the same cell as in (a). (Top of each panel) Spike times are shown as red tricks. (Bottom of each panel) The behavioral timeline is indicated by the distance from the maze center. Prospective and retrospective firing was defined as the reward-related firing before and after the animal entered the arm with the cell's place field. (**c**) Cross-correlogram of spikes with CA3 ripples, demonstrating that spikes mostly occurred in close temporal association with sharp-wave ripple events. (**d**) Reward-associated firing rates of CA3 cells for arm entries before

(prospective), while (field), and after (retrospective) visiting the arm with the place field. There was a significant difference between prospective and retrospective CA3 firing (gray) during reward consumption (0–3 s after the reward onset) at control sites ($n = 39$ cells from 4 animals, prospective vs retrospective, F(1,228) = 6.04, $P = 0.016$, repeated-measures ANOVA) but not lMF sites ($n = 22$ cells from 6 animals, F(1,126) = 0, $P = 0.99$). Corresponding ripple event rates (green) are superimposed on the same graph. While control prospective and retrospective CA3 firing rates differed, there was no change in the ripple rate between prospective and retrospective periods (prospective vs retrospective, control: F(1,456) = 0.21, $P = 0.65$; lMF: F(1,252) = 0.04, $P = 0.85$, repeated-measures ANOVA). Lines with shaded regions are mean ± SEM. (**e**) CA3 ripple-triggered firing rate changes. There was a significant difference between prospective and retrospective CA3 firing during ripples (0–150 ms after the ripple onset) in control group (prospective vs retrospective, F(1,228) = 4.64, $P = 0.034$, repeated-measures ANOVA) but not lMF group (F(1,126) = 0.02, $P = 0.89$). Lines with shaded regions are mean ± SEM. (**f**) (Left) For all CA3 cells, prospective and retrospective firing rates are plotted for spikes during reward (control neurons, black dots; neurons at sites with low-density MF input (lMF), red dots). Many control cells are below the identity line, which indicates higher prospective than restrospective firing (prospective vs retrospective, t(38) = 3.57, $P = 9.8 \times 10^{-4}$, two-sided paired t test). In contrast, the cells from lMF sites scatter around the identity line and do not show a systematic preference (t(21) = 0.97, $P = 0.34$). (Right) The prospective ratio (i.e., prospective firing rate divided by retrospective firing rate) decreased selectively for CA3 neurons with low-density MF input (control vs lMF, t(59) = 2.60, $P = 0.012$; comparison from zero, control: t(38) = 5.09, $P = 1.0 \times 10^{-5}$, two-sided paired t test; lMF: t(21) = 0.57, $P = 0.57$). # $P < 0.05$, comparison from zero within the group; * $P < 0.05$, comparison across the groups. (**g**) Same as in (f), but for the prospective ratio of CA3 firing during reward-associated ripple events (prospective vs retrospective, control: t(38) = 2.15, $P = 0.0077$, two-sided paired t test; lMF: t(21) = 0.13, $P = 0.89$; prospective ratio control vs lMF, t(59) = 1.86, $P = 0.068$; prospective ratio compared from zero, control: t(38) = 2.15, $P = 0.038$, two-sided paired t test; lMF: t(21) = 0.70, $P = 0.49$). # $P < 0.05$.